Survival of the strong, slow, and dense: Field evidence for rapid, transport-dependent bed material abrasion of heterogeneous source lithology

Allison M. Pfeiffer[1], Susannah Morey[2], Hannah M. Karlsson[2], Edward M. Fordham[1], David R. Montgomery[2]

[1] Western Washington University, Geology Department

[2] University of Washington, Department of Earth and Space Science

Key points:

- Abrasion is extremely effective at this site, yet easy to underestimate using standard approaches.
- Source heterogeneity and transport-rate-dependent abrasion largely explain observed downstream trends.
- We present a new method for rapidly quantifying baseline abrasion rate in the field via Schmidt Hammer Rock Strength.

Abstract

Bed material abrasion is a major control on the partitioning of basin-scale sediment fluxes between coarse and fine material. While abrasion is traditionally treated as an exponential function of transport distance and a lithology-specific abrasion coefficient, experimental studies have demonstrated greater complexity in the abrasion process: the rate of abrasion varies with clast angularity, transport rate, and grain size. Yet, few studies have attempted to assess the importance of these complexities in a field setting. Here, we develop a new method for rapidly quantifying baseline abrasion rate in the field via Schmidt Hammer Rock Strength (SHRS). We use this method, along with measurements of gravel bar lithology, to quantify abrasion in the Suiattle River, a basin in the North Cascades of Washington State dominated by a single coarse sediment source: recurrent, debris flows from a tributary draining Glacier Peak stratovolcano. Rapid downstream strengthening of river bar sediment and a preferential loss of weak, low-density vesicular volcanic clasts relative to non-vesicular ones suggest that abrasion is extremely effective in this system. The standard exponential model for downstream abrasion fails to reproduce observed downstream patterns in lithology and clast strength in the Suiattle, despite accounting for the heterogeneity of source material strength and systematic underestimate of abrasion rates by tumbler experiments. Incorporating transport-dependent abrasion into our model largely resolves this failure. While a simplified approach to characterizing abrasion is tempting, our findings show that sediment heterogeneity and transport-dependent abrasion are important controls on the downstream fate of coarse sediment in fluvial systems.

1. Introduction

Coarse sediments in transport along a riverbed gradually reduce in size as a result of grain-to-grain collisions. This process is termed abrasion and represents the combined effects of attrition, the gradual wear of the surface into fine particles, and fragmentation, the loss of larger particles (Attal and Lavé, 2009). Downstream abrasion is commonly modeled as an exponential decay of either the grain diameter or mass,

$$M_x = M_o e^{-\alpha x} \quad [1]$$

where M_o is the original grain mass, M_x is the grain mass at a given distance downstream, x is the downstream transport distance (commonly, in km), and α is a mass loss coefficient (1/km) (Sternberg, 1875). □ is generally defined for a particular lithology either via laboratory experiments (e.g., Attal and Lavé, 2009; O'Connor et al., 2014) or, in early studies, by observed downstream trends in bed material size (e.g., Adams, 1979).

Bed material abrasion shapes both downstream fining and the partitioning of sediment flux between coarse and fine material. Much of the early work on bed material abrasion sought to explain the nearly ubiquitous trend of downstream fining of bed material. Half a century of research has demonstrated that both abrasion and transport processes can produce downstream fining. In the absence of abrasion, downstream fining can be explained by the concavity of river channels and modestly size selective bed material transport (Ferguson et al., 1996; Hoey and Ferguson, 1994), as well as the evolution of river channels to accommodate increasing downstream sediment flux (Gasparini et al., 2004). While durable lithologies (e.g., granite) lose mass too gradually to explain downstream fining in many rivers (Brierley and Hickin, 1991; Ferguson et al., 1996; Lewin and Brewer, 2002), abrasion of more friable lithologies is sufficient

63 to explain the evolution of lithologic mixtures and grain size in other systems (Attal and Lavé,
64 2006).

65 Abrasion is an important control on the partitioning of basin-scale sediment fluxes
66 between coarse and fine material. Durable, abrasion-resistant lithologies tend to be
67 overrepresented in river beds relative to their proportion of the basin area (Attal and Lavé, 2006;
68 Dingle et al., 2017; Mueller et al., 2016), while clasts of friable lithologies rapidly abrade,
69 diminishing their fraction of the bed material and producing silt and clay sized particles in the
70 process (O'Connor et al., 2014). Through this control on coarse sediment flux, abrasion shapes
71 downstream patterns in channel morphology. At the region-scale, O'Connor et al. (2014) found
72 that the distribution of friable marine sedimentary bedrock in western Oregon, USA, controls the
73 distribution of bedrock and alluvial channels, with mainstem bedrock channels found in basins
74 lacking more durable source material. Similarly, Dingle et al. (2017) showed that the
75 downstream limit of coarse sediment effects of landslide pulses in the Himalaya is set by the
76 distance over which abrasion resistant quartzite pebbles break down into sand.

77 While the classic Sternberg (1875) approach to modeling downstream abrasion (Eqn 1) is
78 still commonly employed (e.g., Mueller et al., 2016; O'Connor et al., 2014), its use has several
79 recognized shortcomings. Experimental abrasion apparatuses fail to fully replicate bed material
80 abrasion processes in the field. Barrel tumblers, the most common tool, likely underestimate the
81 rate of abrasion in real rivers by overestimating the effective transport distance in the tumbler,
82 and by failing to create realistic grain to grain impacts (Lewin and Brewer, 2002). Abrasion is
83 generally assumed constant for a given lithology or source material. Yet, several studies have
84 noted that abrasion rate appears to decrease downstream. The weakest individual grains from a
85 sediment source may abrade rapidly downstream from the source, preferentially strengthening

86 the remaining coarse bed sediment. This causes an apparent downstream decrease in the abrasion
87 coefficient measured from bulk bed sediment (Adams, 1979; Sutherland et al., 2002). Multiple
88 studies (Adams, 1979; Dingle et al., 2017), have documented this survivorship bias as reflected
89 in a downstream increase in the ratio of abrasion-resistant quartzite pebbles initiating from sparse
90 veins in source rock to pebbles made of the remainder of the source rock. While quartzite
91 represents only a small fraction of the original source material, it can make up the majority of the
92 bed material at sites tens to hundreds of kilometers downstream. In addition to the preferential
93 survival of strong clasts, rapid abrasion downstream from a sediment source has been explained
94 by efficient abrasion of corners of angular blocks of source material. Termed “phase 1 abrasion”
95 (Domokos et al., 2014), rapid mass loss during initial rounding, followed by more gradual
96 abrasion of rounded particles (“phase 2”), has been demonstrated in models, laboratory
97 experiments (Domokos et al., 2014), and observed in field (Miller et al., 2014). Furthermore,
98 Eqn 1 frames abrasion as a function of transport distance, yet immobile grains are subject to
99 collisions with passing mobile particles, and thus almost certainly abrade in place (Schumm and
100 Stevens, 1973). This immobile-grain abrasion process may be particularly important in coarse
101 headwater streams where both large, immobile boulders and mobile gravel bed material are
102 common. Finally, in Eqn 1 abrasion does not vary with transport rate. Circular flume
103 experiments by Attal and Lavé (2009) demonstrated that abrasion rate increases with particle
104 transport and when grains impact bedrock rather than loose bed material.

105 This study builds on previous research in two ways: by explicitly considering the role of
106 variability in sediment strength, and by accounting for transport-dependent abrasion in our model
107 for the downstream fate of coarse sediment. Models of downstream abrasion have generally
108 relied on laboratory tumbling experiments of bulk sediment mixtures taken in the field to

estimate the abrasion potential of a given sediment source. Such labor-intensive methods limit the feasibility of characterizing variability in sediment abrasion rates within a given source. We hypothesize that this variability acts as an important control on the downstream fate of sediment in a basin. To overcome this limitation, here we develop a new method for rapidly quantifying baseline bed material abrasion rate in the field via Schmidt Hammer Rock Strength (SHRS). We use this new method, along with measurements of gravel bar lithology, to quantify abrasion along the Suiattle River, a basin in the North Cascades of Washington State dominated by a single coarse sediment source: recurrent, debris flows from a tributary draining Glacier Peak stratovolcano. While the transport-dependence of bed material abrasion has been demonstrated in the lab (Attal and Lavé, 2009), to our knowledge, no studies have attempted to either model or corroborate this phenomenon with field observations. Here, we use our detailed observations of source material grain strength, density, and size to model downstream transport-dependent abrasion. This study is made feasible by two particular characteristics of this field site: sediment supply is dominated by a single source, and the supplied sediment consists of two distinct rock types that abrade and transport at different rates.

1.1 Field site

The Suiattle River drains the eastern flank of Glacier Peak, an active stratovolcano in the North Cascades of Washington (Figure 1). Normalized for drainage area, the Suiattle basin contributes about twice as much suspended sediment to the lowland as typical stratovolcano basins in the Pacific Northwest, including those on the west side of Glacier Peak (Czuba et al., 2011; Jaeger et al., 2017). This anomalous sediment load has been attributed to Chocolate Creek (Jaeger et al., 2017), a small tributary rapidly incising a Holocene volcanic apron of lahar and pyroclastic flow material (Beget, 1982). Large mid- to late-20th century debris flows deposited a

>3 m thick, 0.5 km wide fan of unconsolidated volcanic material at the confluence of Chocolate Creek and the Suiattle River (Ford, 1959; Slaughter, 2004). This debris flow material provides a large localized source of volcanic sediment high in the watershed, augmented by lesser debris flow contributions from Dusty Creek, the next tributary downstream (Beget, 1982). Thus, sediment contributions from this small region near the headwaters greatly outweigh downstream tributary inputs, allowing us to consider downstream abrasion of a unified sediment source in the absence of substantial downstream sediment additions. The upper Suiattle River falls within the Glacier Peak Wilderness Area, an area with minimal human impact. There are no dams or sediment control structures in the Suiattle basin, and few roads.

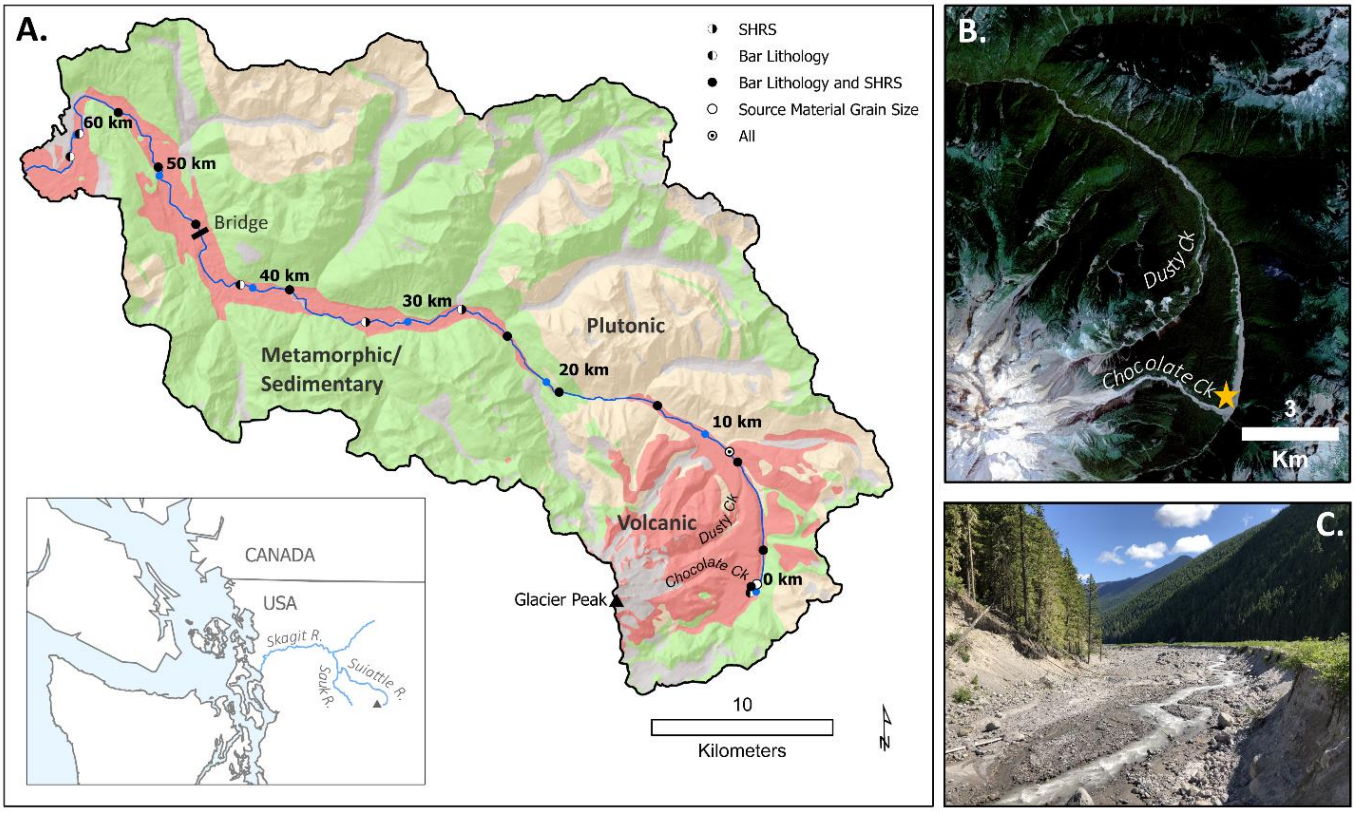

Figure 1. Field Site. (a) Simplified geologic map of the Suiattle basin with field measurement sites marked according to the type of data collected. Downstream distance from Chocolate Creek debris flow deposit marked in blue dots. (b) Satellite imagery of the upper 15 km of the basin (Planet Imagery). (c) Source material debris flow terraces along Chocolate Creek, photo taken at location marked by the star in (b).

2. Methods

To explore downstream bed material abrasion processes in the Suiattle River, we: 1) develop a method to characterize bed material abrasion rate via Schmidt Hammer Rock Strength (SHRS) measurements; 2) characterize the grain size and lithology of the debris flow source material to the Suiattle River; 3) quantify downstream trends in bed surface lithology, SHRS, and grain size along the Suiattle River; and 4) model downstream bed material abrasion.

2.1 A method to characterize abrasion rate via SHRS

Bed material abrasion rate, α (Eqn 1), is typically determined in laboratory experiments using either cylindrical rock tumblers (O'Connor et al., 2014) or annular flumes (Attal et al., 2006). These approaches are time consuming, with tumbling times of hours to days for each sample. Furthermore, rock samples must be transported to the lab. This poses an additional challenge for remote field studies interested in characterizing the abrasion potential of multiple sediment sources. To overcome these challenges, here we present a relationship between Schmidt Hammer Rock Strength (SHRS) and laboratory-determined bed material abrasion rate (α_t).

Schmidt Hammer Rock Strength has been used as a proxy for abrasion potential in geomorphology studies focused on bedrock river incision processes (Duvall, 2004; Murphy et al., 2019), as well as engineering studies focused on the abrasion of dry rock aggregate for construction (Kahraman and Gunaydin, 2007). Reliable measurements of SHRS must be made on samples greater than 11 cm in diameter (Demirdag et al., 2009). However, >11 cm clasts are prohibitively large for tumbler experiments. To overcome this issue, we sampled SHRS of large

cobbles and small boulders along the Suiattle River, then extracted 2-4 smaller subset clasts from these large measured grains, either by rock saw in the lab, or by rock hammer in the field. We measured SHRS $\geq$10 times on each boulder, distributing measurements evenly across smooth surfaces of the clast using a Proceq Rock Schmidt. Here, and elsewhere in this paper, reported SHRS values refer to the median of 10+ measurements on a given clast.

We conducted tumbling experiments to measure the rate of mass loss of individual particles during fluvial transport. Cutting or breaking the sample grains from their original boulders yielded irregularly shaped clasts. Because irregular grains abrade more rapidly than rounded particles (Domokos et al., 2014), we conducted an initial phase of tumbling of each clast until all sharp edges were worn away. Using a tumbling setup similar to that of O'Connor et al. (2014), we filled a rock tumbler with 2.5 kg of sediment and 2 L of water. Each experimental run consisted of a "host" grain size distribution similar to that of gravel patches along the lower mainstem of the Suiattle. The "sample" particles were always a different lithology from the host distribution. For example, plutonic sample particles were tumbled in a host distribution of volcanic sediment. This allowed us to easily distinguish sample particles from the host distribution, and better mimics the mixed-lithology abrasion conditions present in the field. 4-8 sample clasts were included in each run. Sample clasts were grouped to be easily distinguishable by color, size, and shape even if inked sample number labels wore off during a round of tumbling. Starting sample grain mass ranged from 5 to 430 g, with a mean of 126 g.

At the start of each sampling run, we submerged the sample grains in water for 48 hours to allow void spaces to fill with water. We towel-dried and weighed each sample clast, tumbled the grains for 2-20 hours, then dried and weighed them again. Following O'Connor et al. (2014), we converted tumbler experimental time to transport distance using the tumbler revolution rate

and inner circumference of the tumbling barrel, yielding a conversion of 1 hour to 1.15 km of transport. The total duration of tumbling varied with sample strength. We repeated this process until >2% of the original clast mass had abraded, or for at least 50 km of simulated transport. For each clast, we used a best fit regression to calculate the tumbler-derived mass loss coefficient, α_t.

Laboratory methods for quantifying bed material abrasion rate have received criticism (see Lewin and Brewer, 2002) for systematic underestimation of abrasion rates in real rivers. Barrels tend to yield underestimates of bed material abrasion rates, perhaps by a factor of 2-3 or more (Lewin and Brewer, 2002). To correct for this, we explore the use of a tumbler correction factor below.

To calculate clast density, a parameter needed for our transport-dependent abrasion calculations (see below), we measured the volume of each sample clast by displacement of water to the nearest mL.

2.2 Quantifying downstream trends in grain size, lithology, and bed material strength

To characterize the rate of bed material abrasion in the Suiattle, we quantify downstream trends in bed surface grain size, SHRS, and lithology on exposed gravel bars along the Suiattle River between the headwaters and the confluence with the Sauk River (Figure 1).

We measured SHRS and recorded the lithology of ≥50 randomly selected boulders, all of which had a diameter of >11 cm along their smallest axis (the limit for size-independent SHRS measurements, as noted above). We classified the lithology of each boulder as vesicular volcanic, non-vesicular volcanic, volcaniclastic, metamorphic/sedimentary, or plutonic.

In addition to the boulder strength measurements, we quantified bar surface grain size and lithology at 13 sites along the channel. Grains were blindly selected from the bar surface every two steps along repeated transects across the width of the exposed bar. Intermediate grain diameters were measured to the nearest cm. Because many large boulders were partially buried, we measured the diameter of their smallest exposed axis as a proxy for the intermediate grain axis. In our grain size measurements, we excluded fine particles less than 1 cm in diameter. The lithology of each grain was classified using the categories described above. A small number of particles (<1% of all grains measured) were deemed unclassifiable due to their small size.

2.3 Field measurements of source material

The primary source of sediment to the Suiattle River is the debris flow fan at the mouth of Chocolate Creek, with similar terraces at the mouth of Dusty Creek as a possible secondary source. We measured the grain size distribution of the source material in freshly exposed, sub-vertical terraces along Chocolate Creek and the mainstem Suiattle at the Chocolate and Dusty confluences. These terrace exposures were cleaned of loose colluvium to expose a fresh, undisturbed cross section. We measured grains in a 20 cm grid, defined by tape measures hung from the top of the terrace tread. Selected grains were removed from the deposit, and their intermediate axis was measured to the nearest 5 mm. Grains smaller than 5 mm were binned into a single size class. We estimated the intermediate axis diameter of grains that were too large to safely remove, based on their exposed dimensions. The largest grains were occasionally encountered more than once along the grid. These grain diameters were recorded multiple times. At each of the 5 sites we measured the diameter of 50-100 grains. To characterize the abrasion resistance of grains in the deposit, we measured the SHRS of 100 grains within, or in the undisturbed colluvium directly below, fresh terrace faces.

2.4 Predicted downstream abrasion of source material

Here, we take two approaches to modeling the downstream abrasion of the Suiattle source material: first, standard Sternberg mass loss predictions, and second, a calculation of transport-dependent bed material abrasion (Attal and Lavé, 2009).

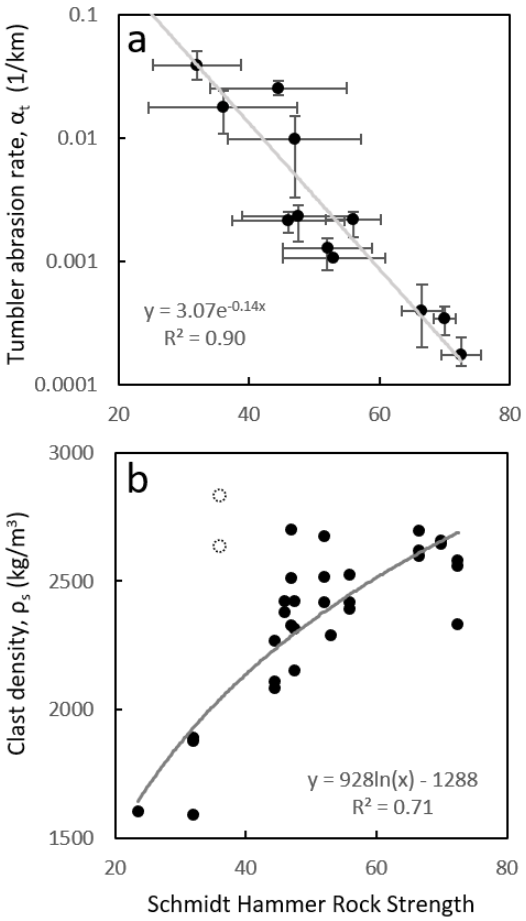

Figure 2. Measured relationship between SHRS and (a) tumbler-derived abrasion rate and (b) wetted-clast density. Horizontal error bars in panel (a) denote the standard deviation of 10+ individual SHRS measurements on a single boulder, while vertical error bars mark the minimum and maximum measured abrasion rate for the 2-4 subset clasts extracted from the boulder. Black dots in figure (b) mark the measured density of individual clasts. The dotted circles denote volcaniclastic samples, which were excluded as outliers from the regression.

2.4.1 Sternberg:

Using the best fit regression in Figure 2a, we calculate a baseline mass-loss abrasion rate for each of the 100 measured boulders in the deposit. We use these α values to predict downstream mass loss for each boulder according to equation 1. Measured downstream changes in lithology on river gravel bars are a reflection of changing proportions of grains by volume, rather than mass. To our knowledge, this fact has thus far been overlooked, as sediment density is often treated as a constant (~2650 kg/m^3). In the Suiattle, though, sediment density varies substantially: at the extreme end of the density spectrum, there are a small number of pumice grains that float found in the deposit. We use the observed relationship between SHRS and clast density (Figure 2b) to predict sediment density for each measured boulder. We predict downstream volume loss over 150 km of transport for each of the 100 grains according to their individual predicted α and density.

2.4.2 Attal:

While Sternberg (1875) remains the standard approach, (Attal and Lavé, 2009) showed that for a given lithology, abrasion rate increases with pebble transport velocity (u_p) at high velocities. According to Sklar and Dietrich (2004):

$$u_p \propto \left(\frac{\rho_s-\rho_w}{\rho_w}\, D \left(\frac{\tau^*}{\tau_c^*}-1\right)\right)^{0.5} \qquad \text{[Eqn 2]}$$

Where ρ_s is sediment density, ρ_w is water density, D is grain diameter, τ^*_c is the dimensionless critical bed shear stress associated with the threshold for grain motion, and τ^* is the dimensionless bed shear stress for a given particle at a given flow, calculated as

$$\tau^* = \frac{\tau}{(\rho_s-\rho_w)gD} \qquad \text{[Eqn 3]}$$

256 τ^*/τ_{*c} is often referred to as transport stage. Based on their finding that abrasion rate scales with

257 u_p^2, Attal and Lavé (2009) propose that

258 $$\alpha \propto \frac{\rho_s - \rho_w}{\rho_w} D \left(\frac{\tau^*}{\tau_c^*} - 1 \right) \qquad \text{[Eqn 4]}$$

259 In Eqn 4, we have retained the densities from Eqn 2, which Attal and Lave (2009) take as

260 constants. They suggest that at lower transport stages (τ^*/τ_{*c} < ~3.3), particle mass loss is higher

261 than this transport-dependent curve due to mobile grains impacting immobile grains on the bed

262 (Figure 3a).

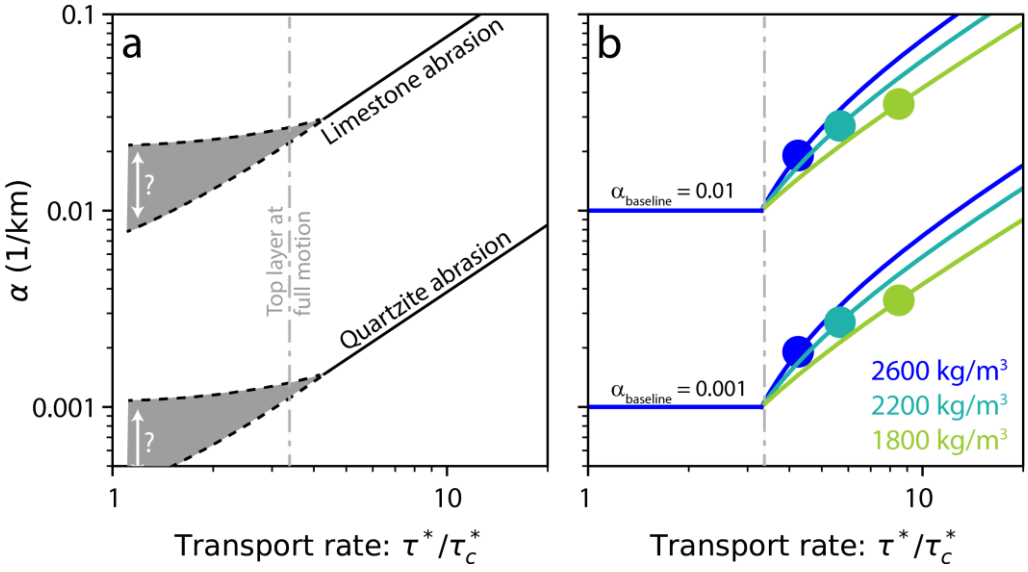

Figure 3 (a) 'Semi-schematic' model of transport-dependent bed material abrasion, modified from Attal and Lave (2009). (b) Representation of transport-dependent bed material abrasion used in this paper (Equation 6), demonstrating the effect of clast density on abrasion rate. Curves are colored by clast density. Dots represent calculated abrasion rates for 40 mm grains of 3 different densities in a 120 Pa flow, k=15, τ^*_c = 0.045.

263

To calculate α for individual grains in the Suiattle, we assume a baseline abrasion rate ($\alpha_{baseline}$) for each grain based on its SHRS using the best-fit regression in Figure 2a, multiplied by a tumbler correction factor, C_t:

$$\alpha_{baseline} = C_t \, \alpha_t \qquad \text{[Eqn 5]}$$

For transport rates >3.3, we calculate abrasion rate as (Figure 3b):

$$\alpha = \alpha_{baseline} \left(1 + k \, \frac{\rho_s - \rho_w}{\rho_w} \, D \left(\frac{\tau^*}{\tau_c^*} - 3.3\right)\right) \qquad \text{[Eqn 6]}$$

Where k is a coefficient that determines the degree of transport-dependence. A k value of 15 approximates the slope of the transport-dependent abrasion relationship described by Attal and Lave (2009). We discuss our choice of k in the results section below.

Predicting downstream sediment abrasion using Eqn 6 requires us to define an initial grain size distribution (GSD) of the source sediment as well as downstream flow characteristics. We assume that all 'parcels' of sediment have the same initial volume, with grain size randomly selected from the measured source GSD and distribution of SHRS. In doing so, we assume that GSD does not vary systematically with lithology.

To assign a transport rate for each parcel of sediment at each downstream point in the channel, we first need to assign τ*. Rather than specifying a particular channel profile and representative flow depth (used to determine τ), or creating a full morphodynamic model that would represent both selective transport and abrasion, we take an abstract approach. The median surface grain size on the upstream most channel bar is 0.14 m. We assume exponential downstream fining in a river channel with a diameter loss coefficient (δ) of 0.01:

$$D_x = D_o \, e^{-\delta x} \qquad \text{[Eqn 7]}$$

Where D_x is the representative grain size at a given distance (x) downstream, and D_o is the starting grain size, in this case 0.14 m. This approach yields downstream patterns that approximately match the fining trends we see in the Suiattle (Supporting Figure 1a), decreasing from a D_{50} of 0.14 m at Chocolate Creek to 0.08 m 62 kilometers downstream, near the confluence with the Sauk. For each downstream distance in the channel, we assume a representative shear stress twice that required to transport D_x of mean sediment density (calculated based on the source material):

$$\tau_x = 2\tau_c^*(\bar{\rho_s} - \rho_w)gD_x \qquad \text{[Eqn 8]}$$

Where we assume $\tau_{*c} = 0.045$, water density $\rho = 1000$ kg/m^3, g = 9.81 m/s^2. This yields plausible dimensional shear stresses of 160 to 37 Pa (Supporting Figure 1b).

We calculate parcel-specific mass loss at each downstream distance from Eqn 6 and Eqn 1, assuming a baseline α and parcel density for each parcel based on SHRS, as above. From parcel-specific mass loss, we calculate downstream changes in parcel volume (V) and grain size:

$$D_x = D_{x-1}\left(\frac{V_x}{V_{x-1}}\right)^{1/3} \qquad \text{[Eqn 9]}$$

Because sand sized grains do not abrade during transport due to viscous damping of grain collisions (Jerolmack and Brzinski, 2010), we set α = 0 for any grains of diameter less than or equal to 0.002 m.

In these abrasion calculations, we make several implicit assumptions. First, we assume that the sediment begins at a single source, with no lateral inputs of sediment and no long-term storage of coarse material in the channel. To the extent that these calculations are intended to model abrasion of volcanic sediment in the Suiattle, we believe this is a reasonable

simplification. Historical accounts and field evidence suggest that Chocolate Creek dominates sediment contributions to the channel, with Dusty Creek (7 km downstream) as a secondary source of occasional volcanic debris flows (Figures 1a and 1b). While there are large boulders within the debris flow terraces, the bed of the Suiattle is not dominated by these boulders (Figure 1c), suggesting that coarse sediment does not remain at the source as a lag deposit. A second assumption in these calculations relates to the products of abrasion. Abrasion represents the combined effects of attrition, which produced clay, silt, and sand sized grains, and fragmentation, which produces larger grains (Kodama, 1994). Here, we assume that the products of abrasion "disappear" from the bed material. We argue that this simplification is reasonable, since fragments tend to be angular, and angular particle abrasion is many times higher than rounded particle abrasion. Furthermore, the fragments tend to be small (Attal and Lavé, 2009), and would thus have high transport rates in subsequent downstream transport, further increasing their rapid transformation to wash load. Finally, in these calculations, we do not include "phase 1" abrasion (Domokos et al., 2014) of angular clasts into rounded ones. Clasts in the debris flow terraces are subrounded, which helps to justify this omission. We consider the implications of this simplification below.

3. Results

3.1 A new method to characterize abrasion rate via SHRS

Our new method for characterizing tumbler-derived abrasion rate via SHRS proves highly effective. In our tumbling experiments, individual clast abrasion rate is well fit by exponential decay, conforming with the classic Sternberg expression for bed material abrasion (Supplementary Figure 2). Comparing these experimentally determined clast abrasion rates to

measured SHRS, we find a strong relationship (Figure 2a). The range of SHRS and abrasion rate sampled here encompasses much of the range of both parameters in natural rocks. We find that clast density varies systematically with SHRS for all but the volcaniclastic sample clasts (Figure 2b).

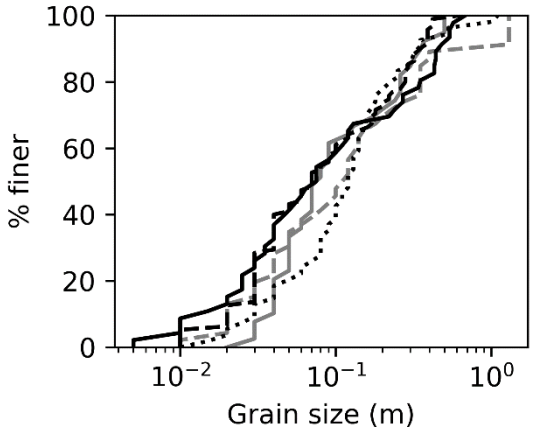

Figure 4. Measured grain size distributions of source material debris flow deposits along the upper Suiattle. Curves represent measurements made at different sites. Dusty Creek terrace measurements in grey, Chocolate Creek terrace measurements in black.

3.2 Field measurements of clast strength, grain size, and lithology

Debris flow deposits in the upper Suiattle are poorly sorted mixtures ranging in size from silt to large boulders (Figure 4). Combining measurements from our 5 sites, the D_{50} of the coarse material (i.e., >2 mm) is 90 mm, with individual site D_{50} between 75 mm and 120 mm. Fine sediment makes up approximately 22% of the deposit. The largest measured grains are 1.3 m, though we note that boulders up to 5 m in diameter can be found scattered throughout the deposit.

The strength (SHRS) of source material boulders varies substantially, from 24 to 73.5, with a median of 52 (Figure 5). Using our calibration curve, this yields a median tumbler-derived abrasion rate of 0.3% per kilometer. Among the measured source material boulders, 81% were vesicular volcanics, and the remaining 19% were non-vesicular volcanics. The vesicular volcanic clasts were systematically weaker than their non-vesicular counterparts, with SHRS between 24 and 65, compared to a range of 47 to 73.

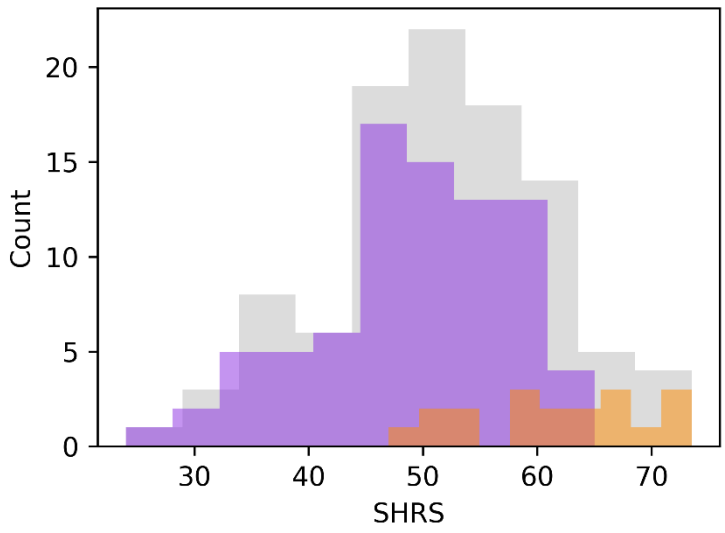

Figure 5. Distribution of measured clast strength within the source deposit. All clasts shown in grey, vesicular volcanics in purple, non-vesicular volcanics in orange.

In the channel, median boulder SHRS increases rapidly over the first 25 km downstream from the source, followed by roughly stable boulder strength in the lower portion of the channel (Figure 6). The rapid downstream strengthening of boulders coincides with an increase in the minimum measured SHRS, but little change in the maximum measured SHRS of boulders.

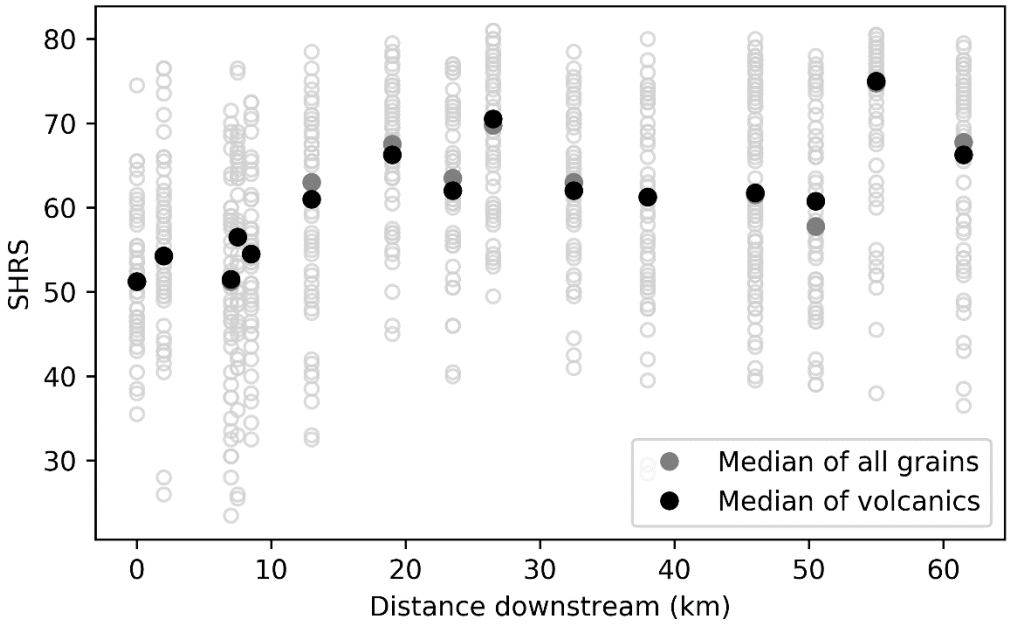

Figure 6. Measured SHRS of clasts on river bars along the Suiattle. All measurements shown in hollow grey circles. The medians of all lithologies at a given bar are marked in grey, the medians of volcanic clasts only are marked in black.

Upstream from the debris flow source zone volcanic clasts make up less than half of the measured grains on the gravel bar (Figure 7). Where the Suiattle incises historic debris flow terraces, the lithology of the gravel bars is dominated by volcanic rocks (95%). Both the fraction of volcanic sediment and the ratio of vesicular to non-vesicular volcanics decrease rapidly in the 20 kilometers immediately downstream from the Chocolate Fan. In the lower 40 km, trends in the volcanic fraction and ratio of vesicular to non-vesicular grains are more subtle. The ratio of vesicular to non-vesicular volcanics varies between 0.8 and 1.6 between 23 km and 46 km. In the lower 10 km of the channel, the ratio of vesicular to non-vesicular volcanics drops and the overall proportion of volcanics decreases, coinciding with a larger portion of plutonic and metasedimentary bed material.

As a check of consistency in our measurements, we can compare the SHRS of volcanic boulders and lithology of bar sediment at the first site incising the Chocolate Creek fan with the SHRS and lithology of boulders in the source deposit. We find good agreement in both median SHRS (51% vs 52%) and the percentage of vesicular volcanics (75% vs 81%). The consistency between source and channel lends support to our assertion that sediment from the Chocolate Creek fan dominates sediment supply in the basin.

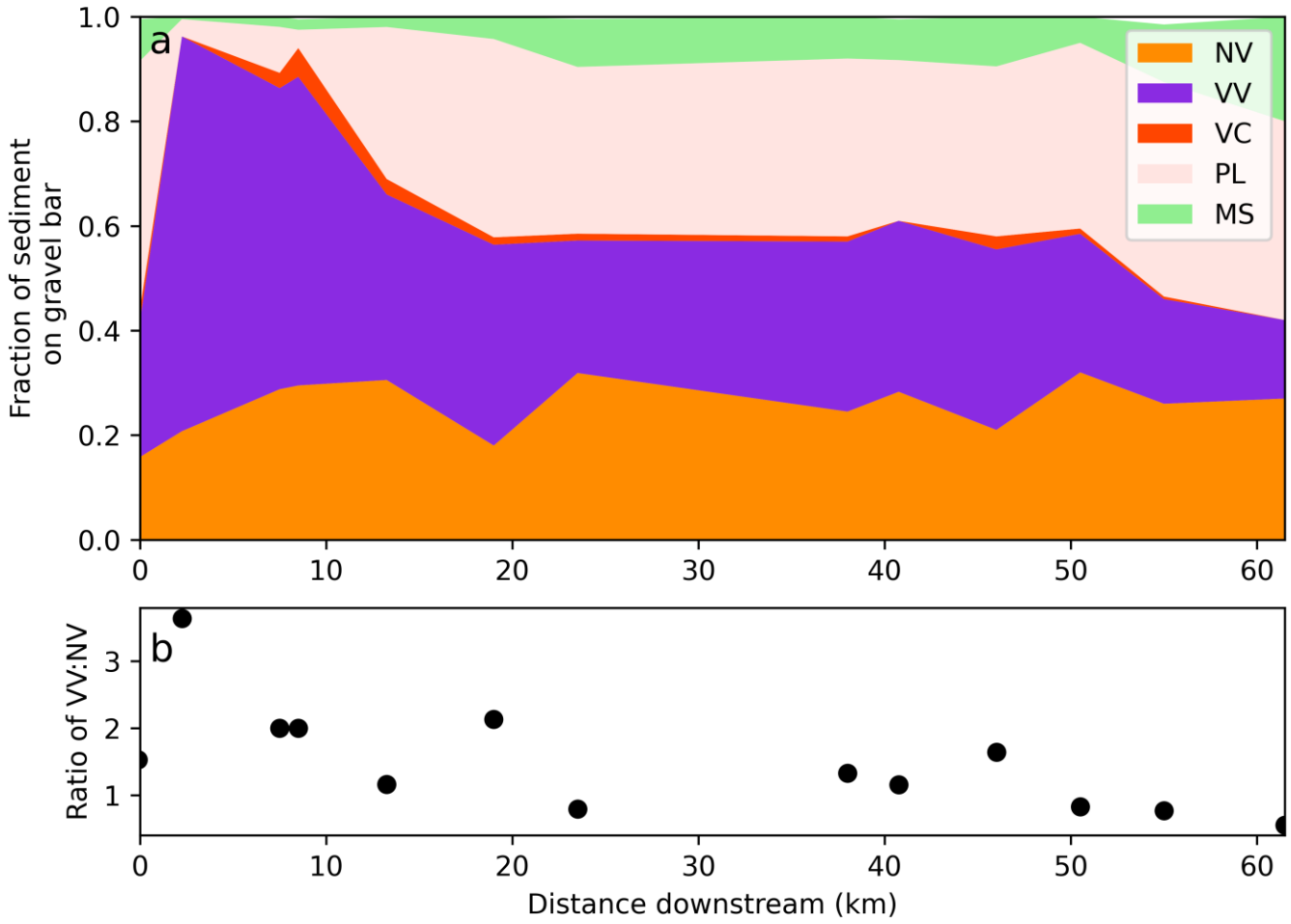

Figure 7. Downstream trends in gravel bar lithology along the Suiattle. (a) Proportions of each lithology category at each downstream site. NV = non-vesicular volcanics, VV = vesicular volcanics, VC = volcaniclastic, PL = Granite and other plutonic rocks, MS = metamorphic and (meta)sedimentary. Unclassified lithologies shown in white, at the top of the stacked plot. (b) Ratio of vesicular to non-vesicular volcanics with distance downstream.

3.3 Modeling downstream abrasion

To quantify the cumulative abrasion potential of the source material sediment, we calculate the predicted volumetric loss of the coarse source material to wash load over 150 km of transport. Assuming simple Sternberg abrasion with an abrasion rate derived from our tumbler experiments and starting clasts of equal volume, we calculate that ~40% of the volume of the coarse source material would be lost to abrasion over 150 km of downstream transport (Figure 8a). In this scenario, abrasion is nearly entirely limited to the non-vesicular fraction of the volcanic source material, with total source material volume gradually lost over the downstream distance. While the weakest clast in the distribution (SHRS = 24, $\alpha_t = 0.12$) is predicted to lose nearly all of its volume over 150 km of transport, the strongest clast (SHRS = 73.5, $\alpha_t = 0.0001$) is predicted to lose only 2% of its volume to abrasion.

To model transport-dependent abrasion, we create a synthetic channel based on an assumed downstream fining rate and transport capacity. Before assessing the implications of transport-dependent abrasion on the downstream loss of the whole distribution (i.e., Figure 8), we consider the predicted transport rates and abrasion of individual clasts.

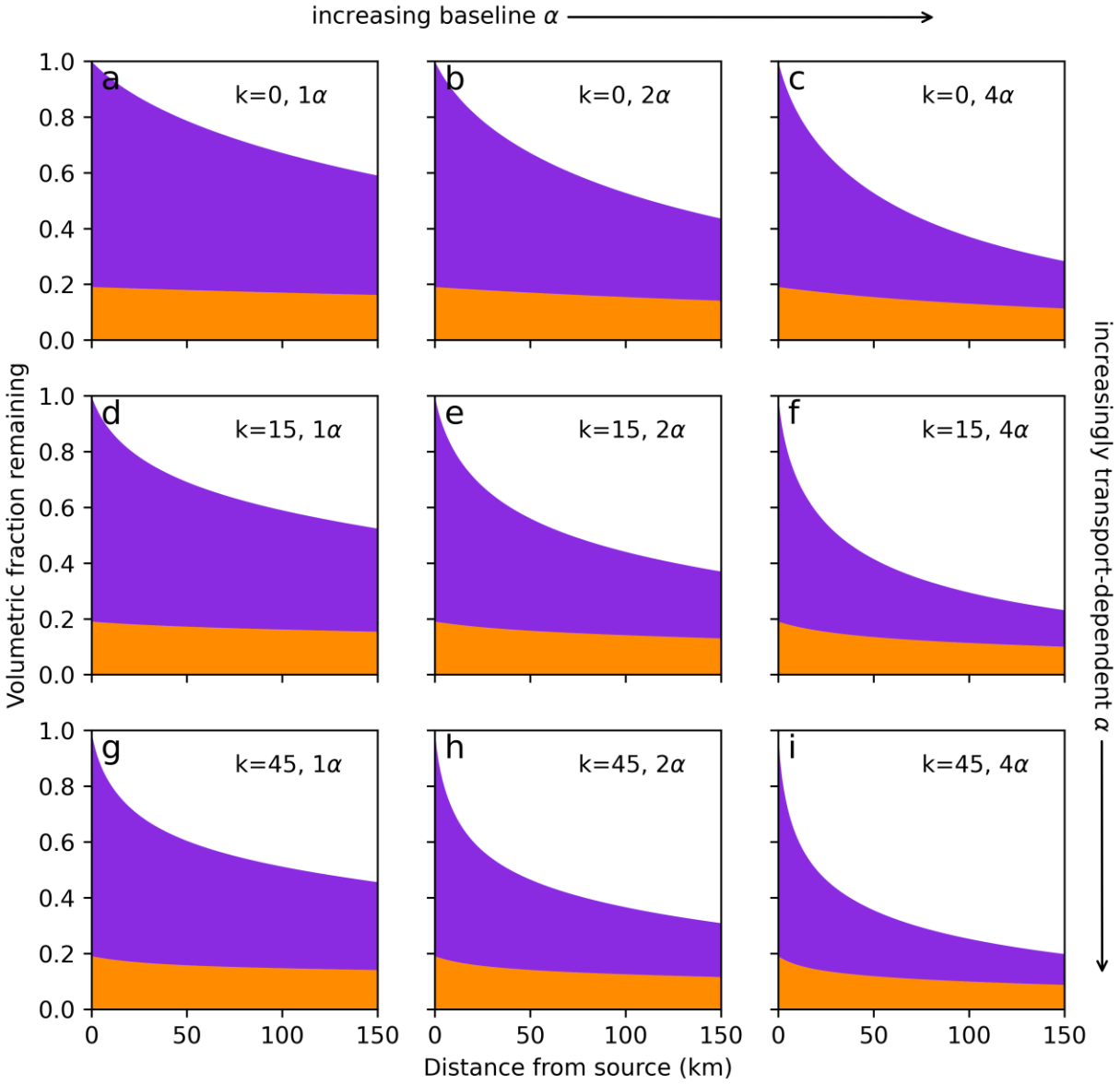

Figure 8. Modeled abrasion of Chocolate Fan sediment over 150 km of downstream transport assuming a variety of transport dependence (k) and tumbler abrasion correction values. As above, vesicular volcanics marked in purple, non-vesicular in orange. Products of abrasion shown in white.

magnitude in the Suiattle, in the case of k = 15, transport-dependent increases in abrasion are responsible for a ~1 order of magnitude increase in α (Figure 9). Rapid transport of grains gives a modest boost to the effectiveness of abrasion, though baseline abrasion rate remains the first order control on α. Because SHRS varies with both abrasion rate and clast density, the weakest grains in our transport model are also the most mobile when normalized for grain size. The small and low density grains are most prone to enhanced, transport-dependent abrasion. Of these highly mobile, high predicted α grains, a small number have transport stages > 30, suggesting that they are transporting in suspension, rarely contacting the bed (Sklar and Dietrich, 2004). In reality, the low frequency of bed contact likely results in a decreased abrasion rate. However, our focus in this paper is on the downstream loss of bed material, making unrealistic abrasion of these small, suspended grains of little consequence to our broader results.

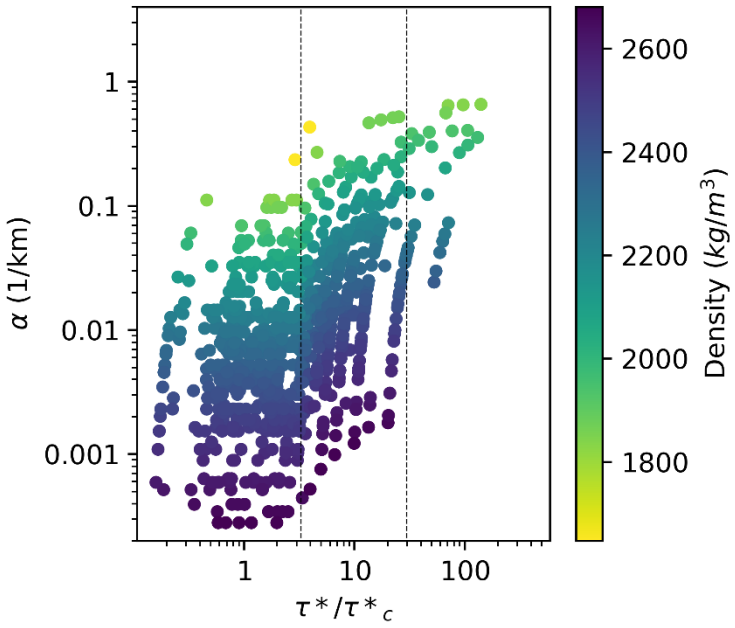

Figure 9. Calculated transport and abrasion rates for 1000 parcels of sediment representing the source material grain size, rock strength, and density distributions, and assuming k = 15 and a tumbler correction factor of 2 at a distance 10 km downstream from the source.

While previous work suggests that the tumbler efficiency parameter (C_t) and the transport dependent abrasion parameter (k) should be greater than 1 and 0, respectively, the literature does not provide us constraints on values for these parameters. Figure 8 explores the sensitivity of downstream abrasion to plausible values of both parameters. As we increase baseline α and transport dependence (k) (Figure 8), predicted loss of coarse source material increases. In all scenarios, this coarse sediment volume loss is dominated by the loss of vesicular volcanics. In the most extreme example modeled here (Figure 8i), we predict loss of 81% of the coarse sediment source to wash load during 150 km of transport. Increases in the tumbler correction factor result in increases in total volume loss downstream. However, the rate of loss remains gradual even in the case of $4\alpha_t$. In contrast, increases in the transport-dependence of abrasion (k) result in rapid loss of source material volume in the first ~25 km downstream from the source.

From these model results we can also calculate downstream changes in the predicted volumetric mean strength of the bulk sediment (Figure 10). In all cases, the mean strength of the bed material increases downstream as a result of the rapid loss of the weakest vesicular volcanic clasts.

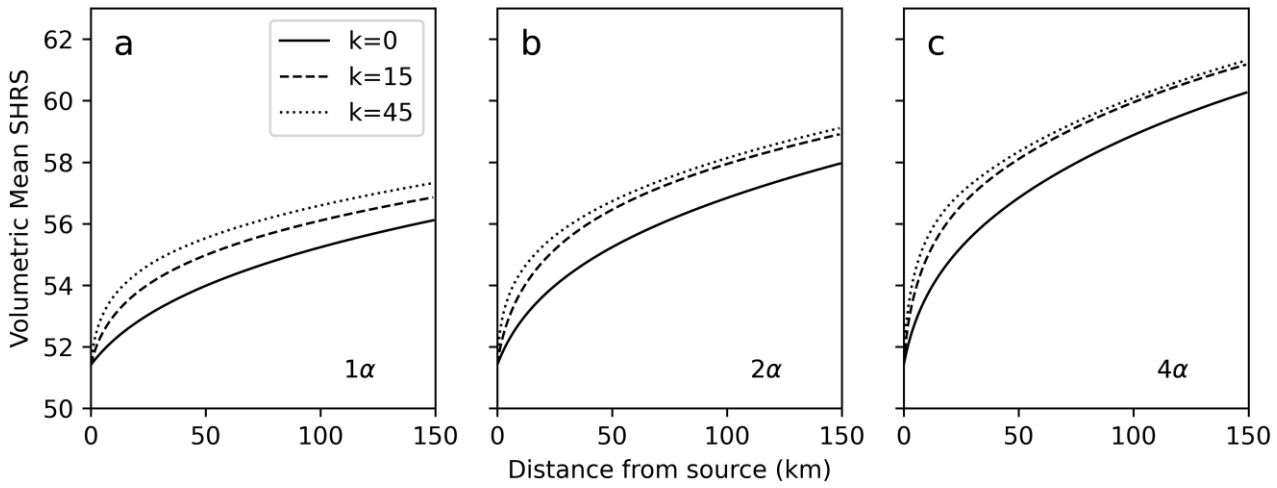

Figure 10. Modeled downstream changes in bed material rock strength. Note the modest increase in modeled SHRS, relative to observations (Figure 6).

4. Discussion

Downstream patterns in gravel bar lithology (Figure 7), combined with the rapid loss of weak grains inferred from the downstream patterns in SHRS (Figure 6), suggest that abrasion processes are extremely effective in the Suiattle River. The abrupt increase in the proportion of volcanic grains at the Chocolate Creek Fan (Figure 7), from ~40% just upstream to 95% at the first site downstream of the introduction of debris flow material, supports our assertion that these debris flow deposits represent a dominant source of sediment in the basin. The rapid loss of weak vesicular volcanics in the subsequent ~15 km, followed by stabilization of the relative lithologic proportions, suggest that while abrasion processes are extremely effective upstream, their effects mellow with downstream distance from the source. This zone of rapid abrasion cannot be easily explained by a bedrock canyon with unusually high transport and abrasion rates: it is a braided river valley.

Comparing these field observations to models for bed material abrasion, we find that transport-dependent abrasion is required to explain the abrupt initial loss in weak vesicular volcanics. In all scenarios of our abrasion model (Figure 8), vesicular volcanics are responsible for the bulk of the downstream loss of coarse sediment. Increases in the baseline α, which represent a greater correction for tumbler efficiency, increase the total predicted volumetric loss over 150 km of transport, but fail to reproduce the abrupt loss of vesicular grains in the first kilometers of transport. Invoking transport-dependence in abrasion yields this abrupt loss, especially in combination with a tumbler efficiency correction of 2-4α_t. While these models of bed material abrasion undoubtedly neglect complexities of the field (e.g., variability in transport rates through time and the abrasion of immobile boulders by mobile impacting grains), the general patterns are instructive. Based on these findings, we suggest that future predictions of

bed material abrasion should invoke a tumbler efficiency correction >1, and transport-dependent abrasion coefficient (k) ~15. Future laboratory tests of the variety conducted by Attal and Lavé (2009) are needed to further constrain these values.

Our model for bed material abrasion falls short in one respect: in all cases, we predict a lower magnitude of bed material strengthening (Figure 10) than we observe in the field. Over the first 25 km downstream from a sediment source, we measured a change in SHRS from 51 to 70. Even our highest-abrasion end member model (dotted line, Figure 10c) predicts a lesser degree of clast strengthening: from 51 to 62 over the full 150 km. Despite this underprediction of the magnitude of downstream strengthening, the rate of strengthening is approximately correct. Both the model and the measurements show rapid initial strengthening over the first 25 km downstream from the sediment source, followed by much more gradual change. This shortcoming suggests that additional abrasion processes are at play that we have not incorporated into our transport-dependent abrasion model. In particular, in-place abrasion processes (Schumm and Stevens, 1973) that preferentially affect large, less-mobile grains may help explain the downstream strengthening of large clasts. More experimental work is needed to inform a quantitative representation of this process.

448 The strong relationship between SHRS and abrasion rate (Figure 2a) presents an easy,
449 and tempting, path forward to predicting downstream abrasion from a few simple field
450 measurements. However, we caution that the simplest versions of this approach are prone to
451 systematically underestimating the magnitude of downstream particle abrasion in several ways.
452 First, the tumbler-based abrasion rate requires a correction factor (C_t), as discussed above.
453 Beyond that, Figure 11 represents five distinct approaches to predicting downstream bed material
454 abrasion in the Suiattle River. The dotted black line represents the simplest approach. Making
455 measurements of boulder SHRS at an easily accessible gravel bar 46 km downstream from the
456 primary sediment source and using the mean SHRS of those boulders to calculate abrasion, we

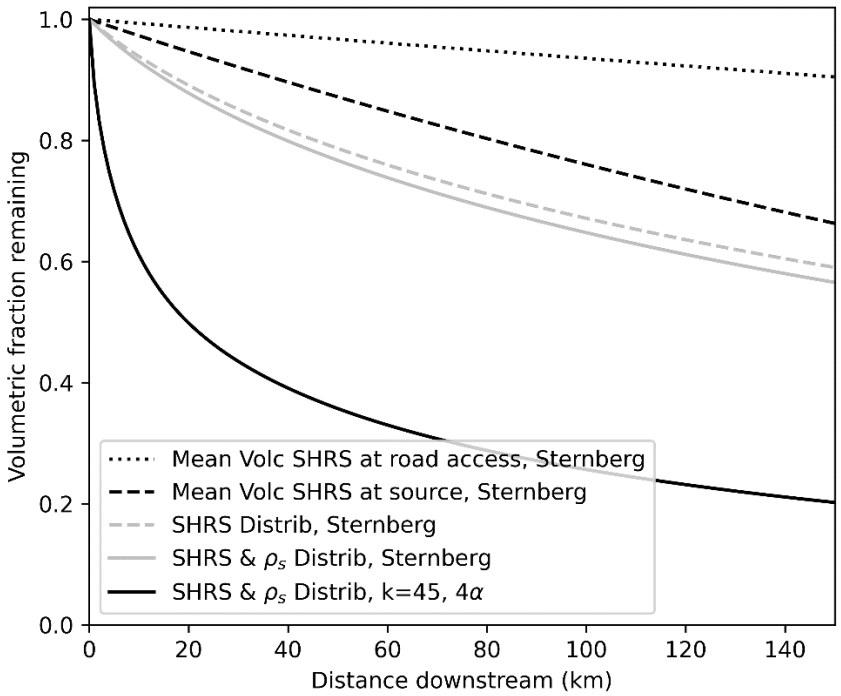

Figure 11. Predictions of downstream abrasion using five different approaches to abrasion prediction. The solid black curve corresponds to the sum of the vesicular and non-vesicular fractions in Figure 8i.

would predict negligible bed material loss of the source material over 150 km of transport (dotted black line, Figure 11). Knowing that the source material is dominated by cobbles and boulders, we might assume that selective transport processes dominate this system, with debris flows leaving large lag deposits of the coarsest material. This first approach fails to account for survivorship bias in downstream transport: the weak clasts are preferentially lost to abrasion. Viewed from the headwaters, abrasion appears to play an important role in the fate of sediment, while viewed from the lower river, abrasion would seem to be negligible. Where source material is heterogeneous, abrasion rate predictions made based on sediment from the lower river will systematically underestimate the abrasion rate upstream of that point. A second tempting approach to abrasion prediction would be to measure SHRS of boulders at the source and use the mean SHRS to estimate downstream abrasion (dashed black line, Figure 11). Using this approach, we predict substantially more abrasion (loss of 35% of the source material over 150 km of transport). A third, more thorough approach would be to calculate the volumetric loss of individual boulders using the distribution of measured SHRS of the source material, assuming a uniform clast density (grey dashed line, Figure 11). This approach yields a prediction of somewhat more rapid volume loss during the first kilometers of downstream transport. Accounting for the variability in clast density yields a small increase in the predicted abrasion (grey solid line, Figure 11). The fourth approach, and the one we advocate for here, accounts for the heterogeneity in source rock strength and density, the underestimate of α_t, and the transport-dependence of abrasion rate (solid black line, Figure 11, identical to Figure 8i). This approach yields a rapid loss of bed material volume in the first 20 km, followed by a gradual decline. The five methods depicted in Figure 11 represent a continuum of complexity in quantifying bed material abrasion processes. We find that the simplest, and most commonly employed (e.g.

480 Ferguson et al., 1996; O'Connor et al., 2014), approaches systematically underpredict the
481 magnitude of downstream abrasion in a river with heterogeneous source material.

482 While our approach to predicting downstream abrasion (solid black line, Figure 11) better
483 reproduces the observed patterns in downstream lithology than a standard approach (dotted black
484 line, Figure 11), there are several components to the abrasion process that we have not
485 represented. While transport-dependent abrasion will tend to enhance the downstream loss of
486 finer and lower-density particles, there are two potentially important abrasion processes that may
487 enhance the abrasion of coarse particles that we have not represented. First, Attal and Lave noted
488 that larger grains tend to abrade at a higher rate. This is represented in our model as an increase
489 in α with D in equation 9. In this representation, α is insensitive to grain size below $\tau^*/\tau_{*c} = 3.3$.
490 The experiments by Attal and Lave are inconclusive as to the sensitivity of abrasion rate to grain
491 size at low transport rates. Lacking more quantitative constraints on the relationship between
492 lithologic strength, grain size, and baseline abrasion, we have not attempted to include this in our
493 model. However, this grain size dependence may be important in the Suiattle, with its poorly
494 sorted source grain mixture. Second, immobile grains will abrade in place as they are impacted
495 by passing mobile grains (Schumm and Stevens, 1973). While this component of the abrasion
496 process has been long recognized, to our knowledge no quantitative representations for the
497 process exist. This sedentary abrasion will increase the mass loss per kilometer of transport for
498 large and dense grains that transport slowly, resulting in mass loss that is rapid in space but slow
499 in time when compared to the abrasion of small, highly mobile grains. Both of these abrasion
500 mechanisms neglected in our model have the potential to help resolve our failure to reproduce
501 the observed magnitude of downstream clast strengthening (Figures 6 and 10).

Historically, much of the literature on bed material abrasion has focused on downstream fining. Here, our focus has been on abrasion-set controls on downstream coarse sediment flux, rather than the relative importance of abrasion and selective transport in downstream fining. However, our findings have potentially intriguing implications for bed material morphodynamics of heterogeneous material. The low density, weak grains shrink in diameter rapidly downstream due to their high baseline abrasion rate and the enhanced transport-dependent abrasion promoted by the low clast density. The downstream reduction in size further enhances both transport rate and transport-dependent abrasion, suggesting a transport feedback with abrasion in low-strength clasts. These effects have intriguing implications for sediment pulse transfer in weak or heterogeneous sediments. Tackling these questions would require a Lagrangian morphodynamic model that individually tracks the downstream evolution of parcels of sediment of varying abrasion rate, density, and size.

Geomorphologists are likely to treat sediment from a constrained source as a uniform lithology, assuming a single abrasion rate (e.g., O'Connor et al., 2014). Our findings demonstrate the peril of this approach. Stratovolcanoes, such as the source zone of our study area, are particularly prone to the problem of easily underestimated bed material abrasion, given the wide range of tephra rock strength and clast density. These volcanoes are also the source of enormous sediment pulses: volcanic eruptions, lahars, and catastrophic rock avalanches (Friele and Clague, 2009; Geertsema et al., 2006). Predicting abrasion rate is important in these settings because the downstream hazard of coarse sediment (e.g., increased flooding due to channel aggradation (Slater et al., 2015) are different from downstream hazards associated with the fine sediment products of abrasion (e.g., habitat degradation (Greig et al., 2005)).

Heterogeneous baseline abrasion rates are not limited to stratovolcanoes, however. Some sedimentary rock units and metamorphic mélanges are likely quite heterogeneous as well. In a study of sediment pulse transfer in the Navarro River of Northern California, Sutherland et al. (2002) found an apparent reduction in α over time during their abrasion experiments of landslide deposits consisting of a mix of sandstone, siltstone, and mudstone. This can be explained by a preferential loss of weak clasts early in the experiment. Their results mirror our finding of rapid downstream clast strengthening in the Suiattle. We are not the first to recognize the role of survivorship bias in sediment abrasion (Adams 1979), but the importance of this phenomena seems to be frequently overlooked.

5. Conclusion

Our site, with its heterogeneous source material from a localized headwater source, combined with our SHRS method to quantify the relative abrasion potential of source and bed material, provide us a rich dataset with which to test our existing understanding of bed material abrasion processes. The standard exponential model for downstream abrasion fails to reproduce observed downstream patterns in lithology and clast strength in the Suiattle, even when accounting for the heterogeneity of source material strength and systematic underestimate of abrasion rates by tumbler experiments. Incorporating transport-dependent abrasion into our model largely resolves this failure, though the magnitude of downstream strengthening of coarse material remains lower in our models than we measure in the field. This shortcoming hints at further complexities in the abrasion process for which we lack quantitative process descriptions.

Acknowledgements

We thank Selina Davila Olivera, Jaycob Davies, Riley Keister, Vivien McNett, Stephen Novak, and Ana Zissou for assistance in the field, and Gabe Gordon, JoJo Mangano, and Jim O'Connor for use of the rock tumbler. Funding for this work was provided by Western Washington University, the Quaternary Research Center at the University of Washington, an NCED II, Postdoctoral Fellowship (to A. Pfeiffer), and NSF PREEVENTS program (ICER 1663859). We are in the process of archiving the data for this manuscript on PANGAEA, a data archive repository that meets the FAIR data requirements. In the interim, we have attached the data as a temporary supplementary document.

References

Adams J. 1979. Wear of unsound pebbles in river headwaters. Science **203** : 171–172. DOI: 10.1126/science.203.4376.171.

Attal M, Lavé J. 2006. Changes ofbedload characteristics along the Marsyandi River (central Nepal): Implications for understanding hillslope sediment supply, sediment load evolution along. Tectonics, climate, and landscape evolution **2398** : 143–171. DOI: 10.1130/2006.2398(09).

Attal M, Lavé J. 2009. Pebble abrasion during fluvial transport: Experimental results and implications for the evolution of the sediment load along rivers. Journal of Geophysical Research: Earth Surface **114** : 1–22. DOI: 10.1029/2009JF001328.

Attal M, Lavé J, Masson J-P. 2006. New facility to study river abrasion processes. Journal of Hydraulic Engineering **132** : 624–628.

Beget JE. 1982. Postglacial volcanic deposits at Glacier Peak, Washington, and potential hazards from future eruptions. U.S. Geological Survey Open-File Report 82-830, 77 p.

Brierley GJ, Hickin EJ. 1991. Channel planform as a non-controlling factor in fluvial sedimentology: the case of the squamish river floodplain, British Columbia. Sedimentary Geology **75** : 67–83. DOI: 10.1016/0037-0738(91)90051-E

Czuba JA, Magirl CS, Czuba CR, Grossman EE, Curran CA, Gendaszek AS, Dinicola RS. 2011. Sediment Load from Major Rivers into Puget Sound and its Adjacent Waters. U.S. Geological Survey Fact Sheet 2011-3083, 4 p.

576 Demirdag S, Yavuz H, Altindag R. 2009. The effect of sample size on Schmidt rebound hardness
577 value of rocks. International Journal of Rock Mechanics and Mining Sciences **46** : 725–730.
578 DOI: 10.1016/j.ijrmms.2008.09.004.

579 Dingle EH, Attal M, Sinclair HD. 2017. Abrasion-set limits on Himalayan gravel flux. Nature
580 **544** : 471–474. DOI: 10.1038/nature22039.

581 Domokos G, Jerolmack DJ, Sipos AÁ, Török Á. 2014. How River Rocks Round: Resolving the
582 Shape-Size Paradox. Magar V (ed). PLoS ONE **9** : e88657. DOI: 10.1371/journal.pone.0088657.

583 Duvall A. 2004. Tectonic and lithologic controls on bedrock channel profiles and processes in
584 coastal California. Journal of Geophysical Research **109** : F03002. DOI: 10.1029/2003JF000086.

585 Ferguson R, Hoey T, Wathen S, Werritty A. 1996. Field evidence for rapid downstream fining of
586 river gravels through selective transport. Geology **24** : 179–182. DOI: 10.1130/0091-
587 7613(1996)024<0179:FEFRDF>2.3.CO;2.

588 Ford AB. 1959. Geology and petrology of the Glacier Peak quadrangle, northern Cascades,
589 Washington: Seattle, University of Washington, PhD Thesis, Ph. D. dissertation.

590 Friele PA, Clague JJ. 2009. Paraglacial geomorphology of Quaternary volcanic landscapes in the
591 southern Coast Mountains, British Columbia. Geological Society, London, Special Publication
592 **320** : 219–233. DOI: 10.1144/SP320.14.

593 Gasparini NM, Tucker GE, Bras RL. 2004. Network-scale dynamics of grain-size sorting:
594 Implications for downstream fining, stream-profile concavity, and drainage basin morphology.
595 Earth Surface Processes and Landforms **29** : 401–421. DOI: 10.1002/esp.1031.

596 Geertsema M, Clague JJ, Schwab JW, Evans SG. 2006. An overview of recent large catastrophic
597 landslides in northern British Columbia, Canada. Engineering Geology **83** : 120–143. DOI:
598 10.1016/j.enggeo.2005.06.028.

599 Greig SM, Sear DA, Carling PA. 2005. The impact of fine sediment accumulation on the
600 survival of incubating salmon progeny: Implications for sediment management. Science of The
601 Total Environment **344** : 241–258. DOI: 10.1016/j.scitotenv.2005.02.010.

602 Hoey TB, Ferguson R. 1994. Numerical simulation of downstream fining by selective transport
603 in gravel bed rivers: Model development and illustration. Water Resources Research **30** : 2251–
604 2260. DOI: 10.1029/94WR00556.

605 Jaeger KL, Curran CA, Anderson SW, Morris ST, Moran PW, Reams KA. 2017. Suspended
606 sediment, turbidity, and stream water temperature in the Sauk River Basin, western Washington,
607 water years 2012-16. U.S. Geological Survey Scientific Investigations Report 2017–5113 : 47.
608 DOI: 10.3133/sir20175113.

609 Jerolmack DJ, Brzinski TA. 2010. Equivalence of abrupt grain-size transitions in alluvial rivers
610 and eolian sand seas: A hypothesis. Geology **38** : 719–722. DOI: 10.1130/G30922.1.

611 Kahraman S, Gunaydin O. 2007. Empirical methods to predict the abrasion resistance of rock
612 aggregates. Bulletin of Engineering Geology and the Environment **66** : 449–455. DOI:
613 10.1007/s10064-007-0093-2.

614 Kodama Y. 1994. Experimental study of abrasion and its role in producing downstream fining in
615 gravel-bed rivers. Journal of Sedimentary Research **64** : 76–85. DOI: 10.2110/jsr.64.76.

Lewin J, Brewer PA. 2002. Laboratory simulation of clast abrasion. Earth Surface Processes and Landforms: The Journal of the British Geomorphological Research Group **27** : 145–164.

Miller KL, Szabó T, Jerolmack DJ, Domokos G. 2014. Quantifying the significance of abrasion and selective transport for downstream fluvial grain size evolution. Journal of Geophysical Research: Earth Surface **119** : 2412–2429. DOI: 10.1002/2014JF003156.

Mueller ER, Smith ME, Pitlick J. 2016. Lithology-controlled evolution of stream bed sediment and basin-scale sediment yields in adjacent mountain watersheds, Idaho, USA. Earth Surface Processes and Landforms **1883** : 1869–1883. DOI: 10.1002/esp.3955.

Murphy BP, Czuba JA, Belmont P. 2019. Post-wildfire sediment cascades: A modeling framework linking debris flow generation and network-scale sediment routing. Earth Surface Processes and Landforms **44** : 2126–2140. DOI: 10.1002/esp.4635.

O'Connor JE, Mangano JF, Anderson SW, Wallick JR, Jones KL, Keith MK. 2014. Geologic and physiographic controls on bed-material yield, transport, and channel morphology for alluvial and bedrock rivers, western Oregon. Bulletin of the Geological Society of America **126** : 377–397. DOI: 10.1130/B30831.1.

Schumm SA, Stevens MA. 1973. Abrasion in place: A mechanism for rounding and size reduction of coarse sediments in rivers. Geology **1** : 37-40.

Sklar LS, Dietrich WE. 2004. A mechanistic model for river incision into bedrock by saltating bed load. Water Resources Research **40** : n/a–n/a. DOI: 10.1029/2003WR002496.

635 Slater LJ, Singer MB, Kirchner JW. 2015. Hydrologic versus geomorphic drivers of trends in
636 flood hazard. Geophysical Research Letters **42** : 370–376. DOI: 10.1002/2014GL062482.

637 Slaughter SL. 2004. The 1938 Chocolate Glacier Debris Flow, Glacier Peak Volcano, North
638 Cascades, Washington (Master's Thesis), Master's Thesis, Ellensburg, WA: Central Washington
639 University.

640 Sternberg H. 1875. Untersuchungen uber Langen-und Querprofil geschiebefuhrender Flusse.
641 Zeitshrift fur Bauwesen **25** : 483–506.

642 Sutherland DG, Ball MH, Hilton SJ, Lisle TE. 2002. Evolution of a landslide-induced sediment
643 wave in the Navarro River, California. Bulletin of the Geological Society of America **114** :
644 1036–1048. DOI: 10.1130/0016-7606(2002)114<1036:EOALIS>2.0.CO;2.

645

Figure 10.

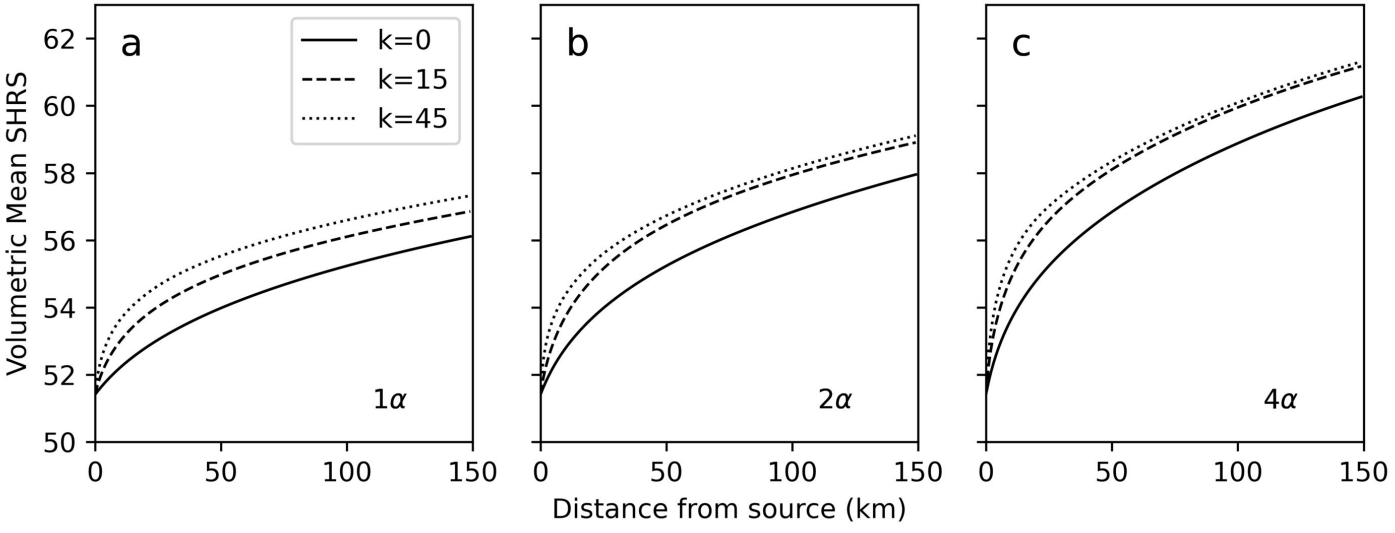
a
b
c
k=0
k=15
k=45
1α
2α
4α
Volumetric Mean SHRS
Distance from source (km)
62
60
58
56
54
52
50
0
50
100
150

Figure 11.

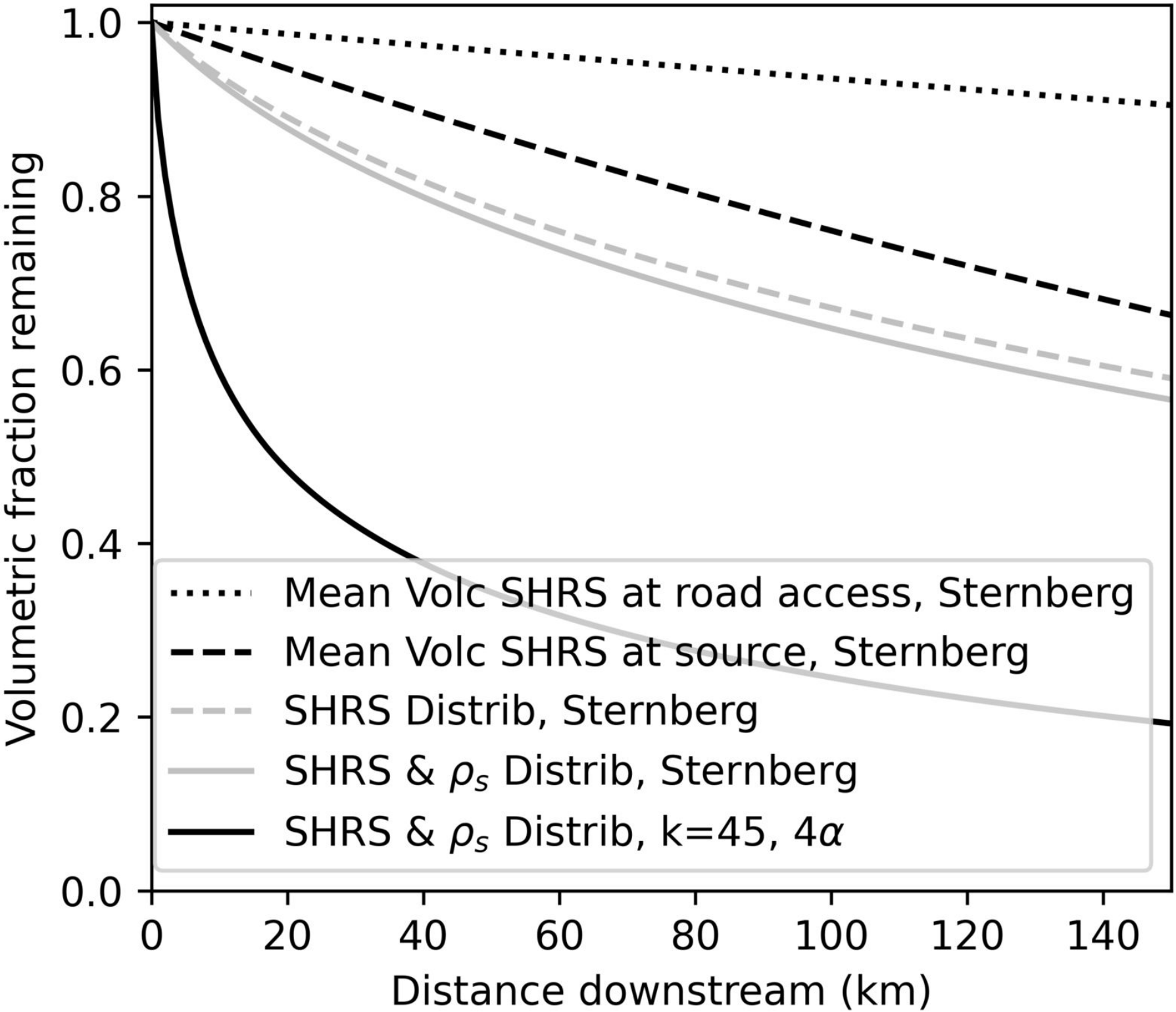
1.0
0.8
0.6
0.4
0.2
0.0
Volumetric fraction remaining
0
20
40
60
80
100
120
140
Distance downstream (km)
Mean Volc SHRS at road access, Sternberg
Mean Volc SHRS at source, Sternberg
SHRS Distrib, Sternberg
SHRS & ρ_s Distrib, Sternberg
SHRS & ρ_s Distrib, k=45, 4α

Figure 1.

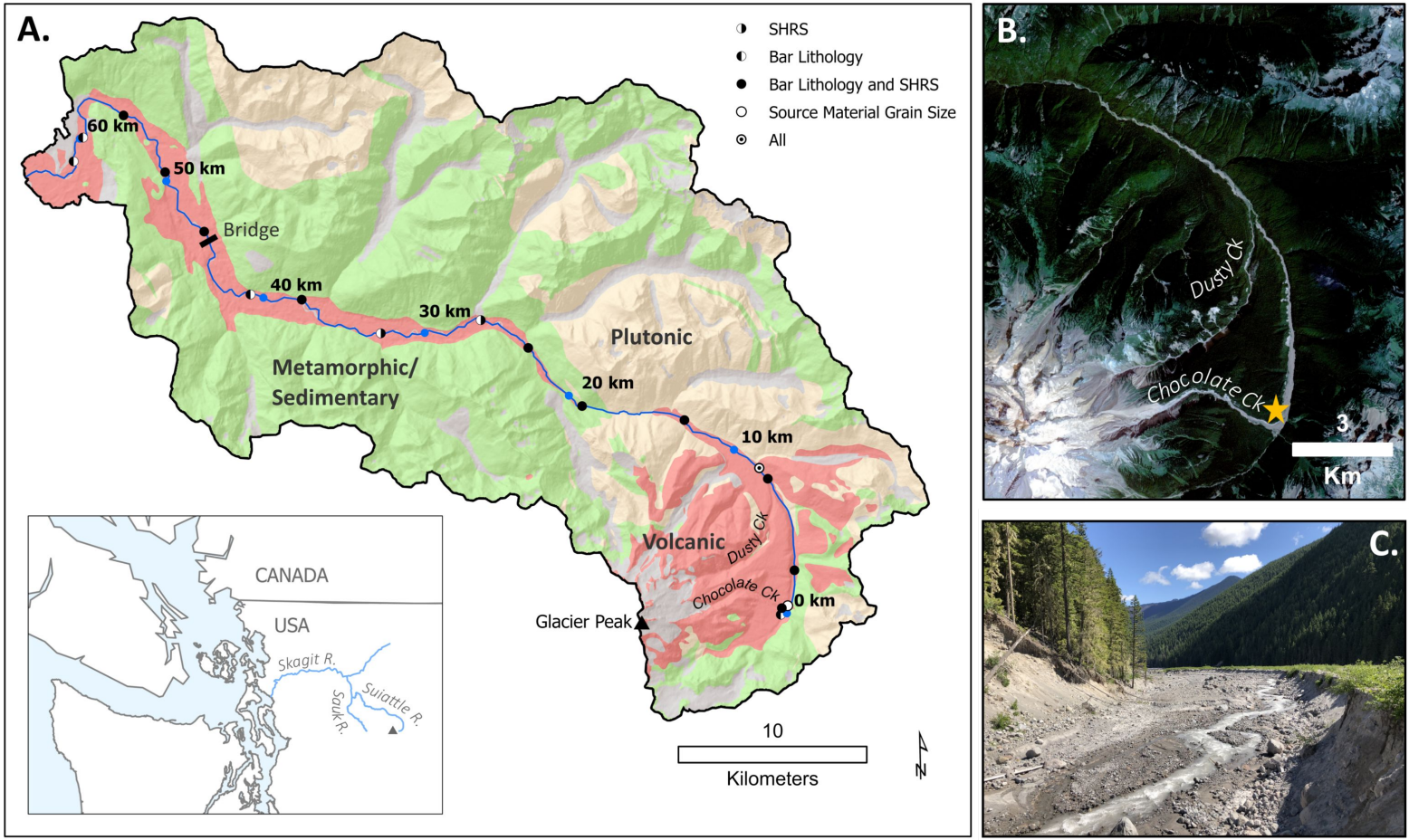
A.
SHRS
Bar Lithology
Bar Lithology and SHRS
Source Material Grain Size
All
60 km
50 km
Bridge
40 km
30 km
20 km
10 km
0 km
Plutonic
Metamorphic/
Sedimentary
Volcanic
Dusty Ck
Chocolate Ck
Glacier Peak
10
Kilometers
N
CANADA
USA
Skagit R.
Sauk R.
Suiattle R.
B.
Dusty Ck
Chocolate Ck
3
Km
C.

Figure 2.

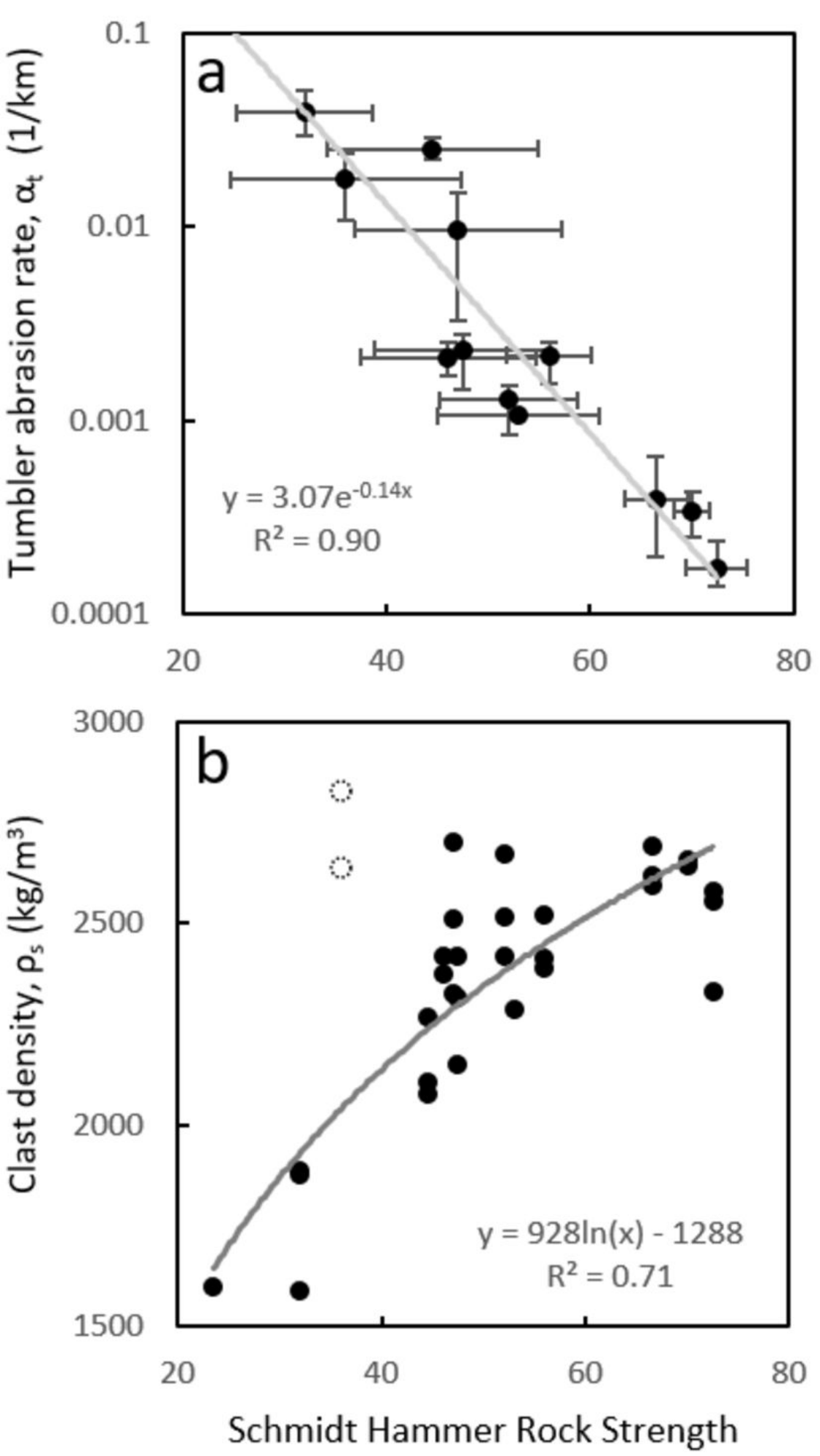
a
Tumbler abrasion rate, α_t (1/km)
0.1
0.01
0.001
0.0001
y = 3.07e^-0.14x
R² = 0.90
20
40
60
80
b
Clast density, ρ_s (kg/m³)
3000
2500
2000
1500
y = 928ln(x) - 1288
R² = 0.71
20
40
60
80
Schmidt Hammer Rock Strength

Figure 3.

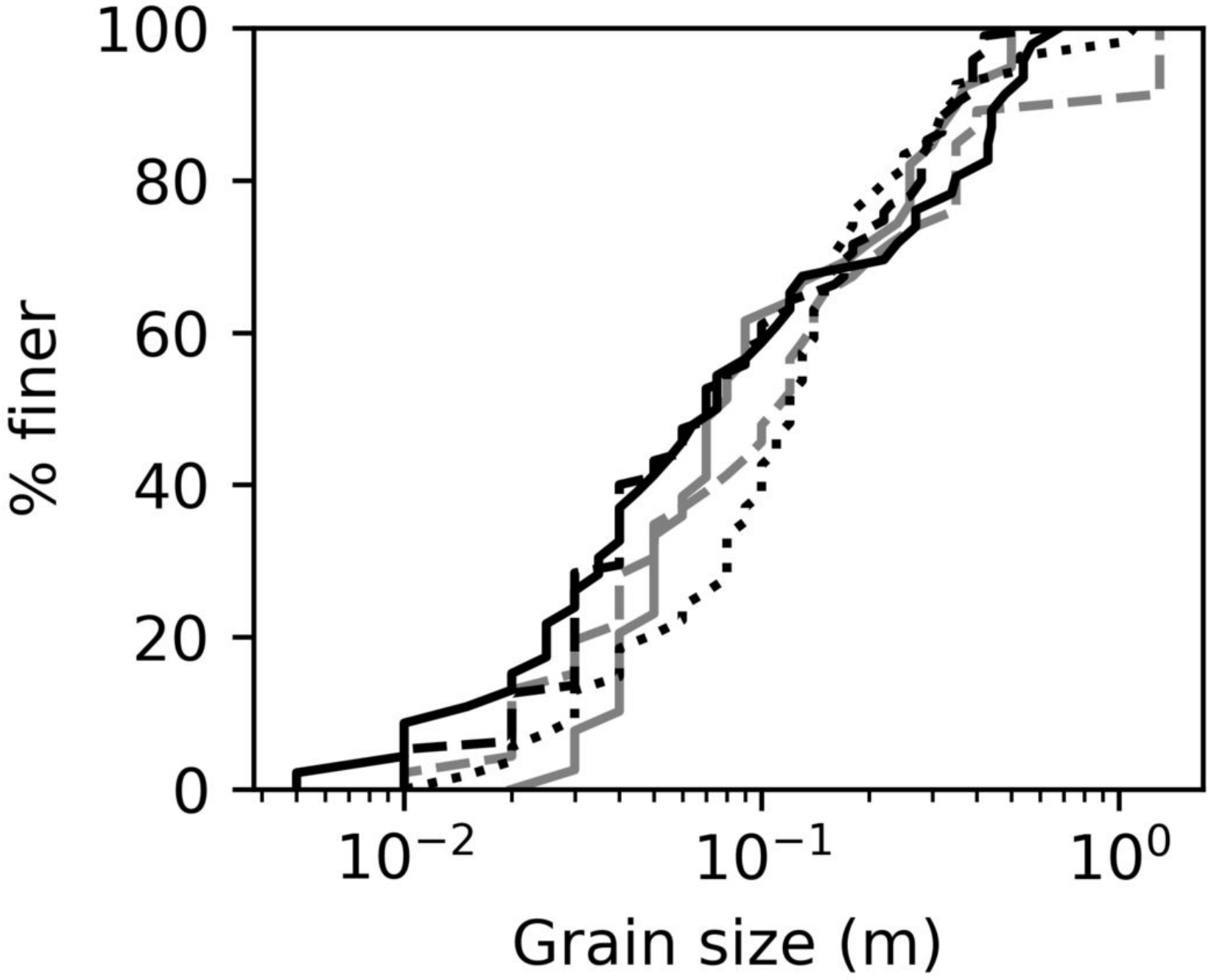
100
80
60
40
20
0
% finer
10^{-2}
10^{-1}
10^{0}
Grain size (m)

Figure 4.

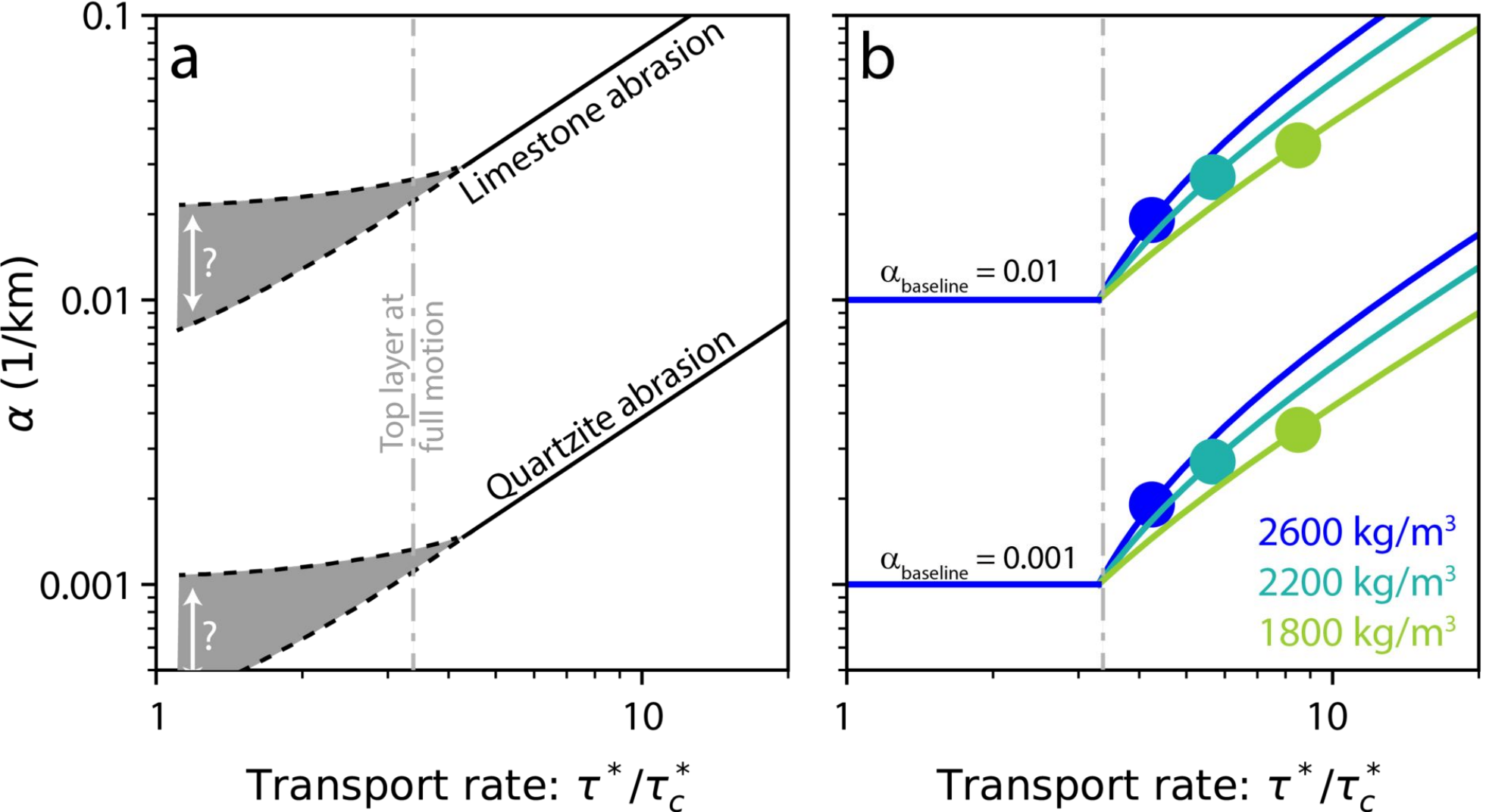
a
b
0.1
0.01
0.001
α (1/km)
Limestone abrasion
Quartzite abrasion
Top layer at full motion
?
?
1
10
Transport rate: τ^*/τ_c^*
$\alpha_{baseline} = 0.01$
$\alpha_{baseline} = 0.001$
2600 kg/m³
2200 kg/m³
1800 kg/m³

Figure 5.

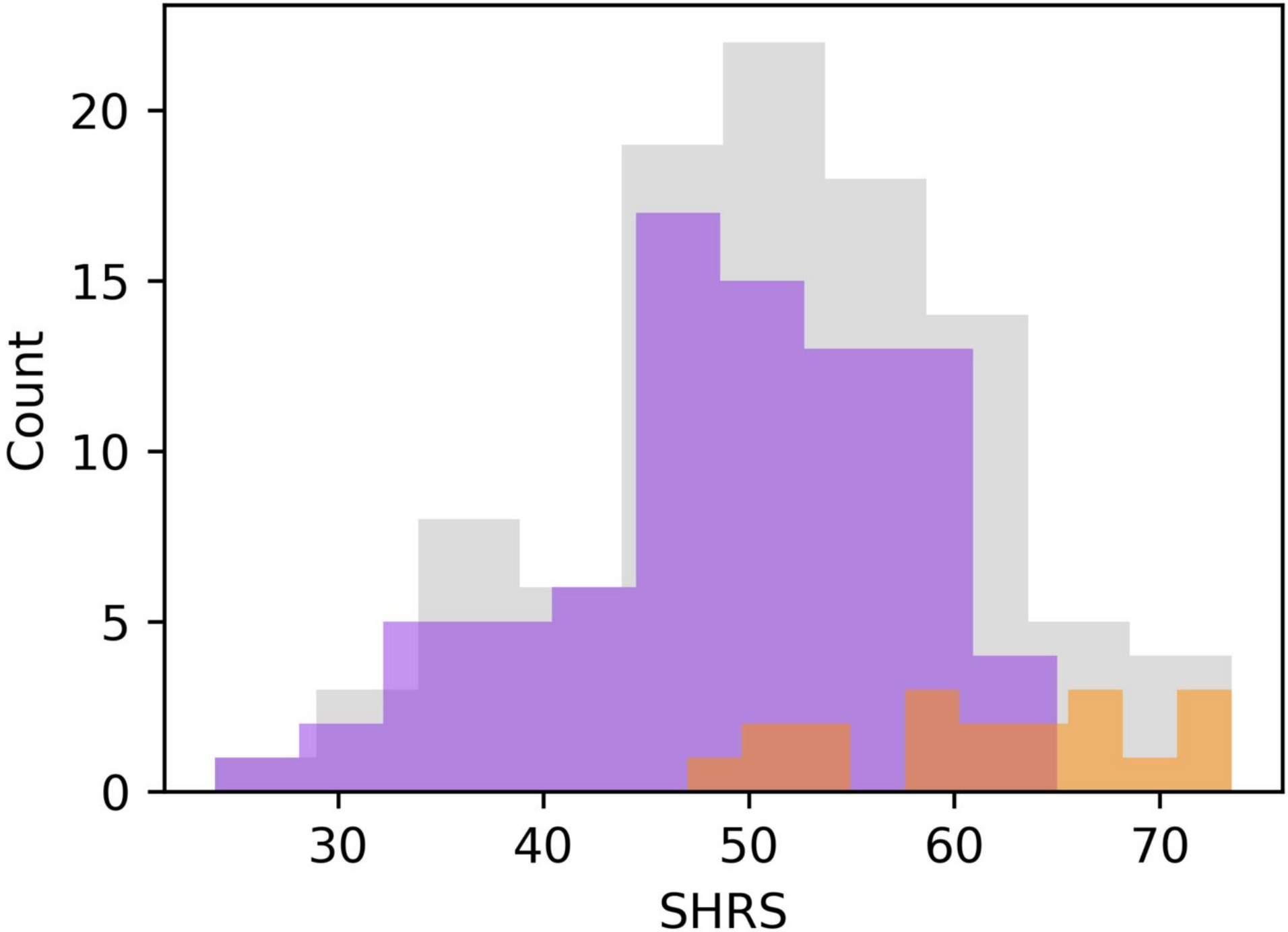
Count
0
5
10
15
20
30
40
50
60
70
SHRS

Figure 6.

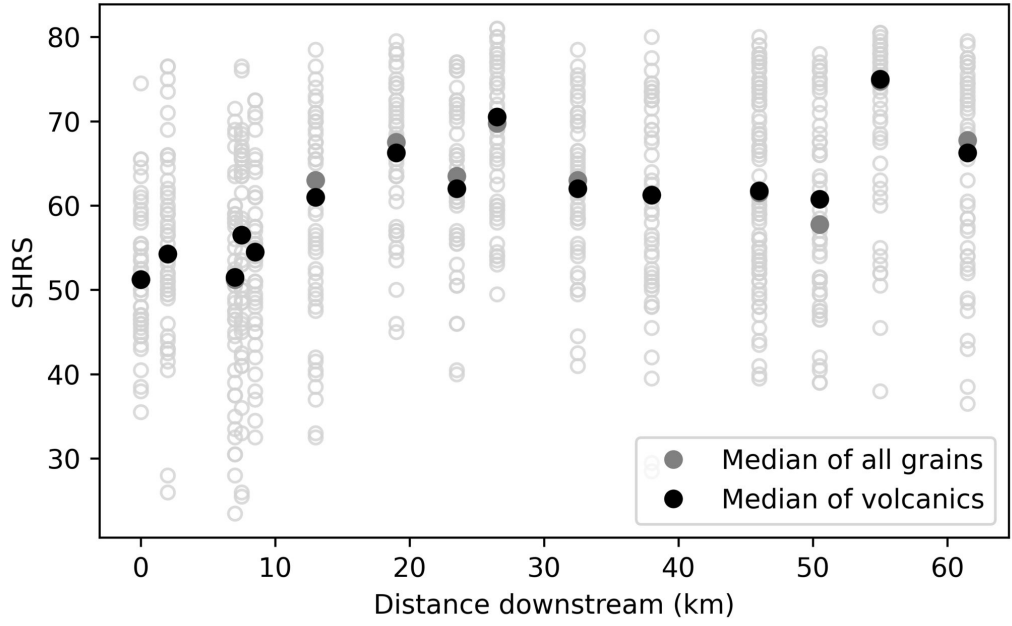
SHRS
80
70
60
50
40
30
0
10
20
30
40
50
60
Distance downstream (km)
Median of all grains
Median of volcanics

Figure 7.

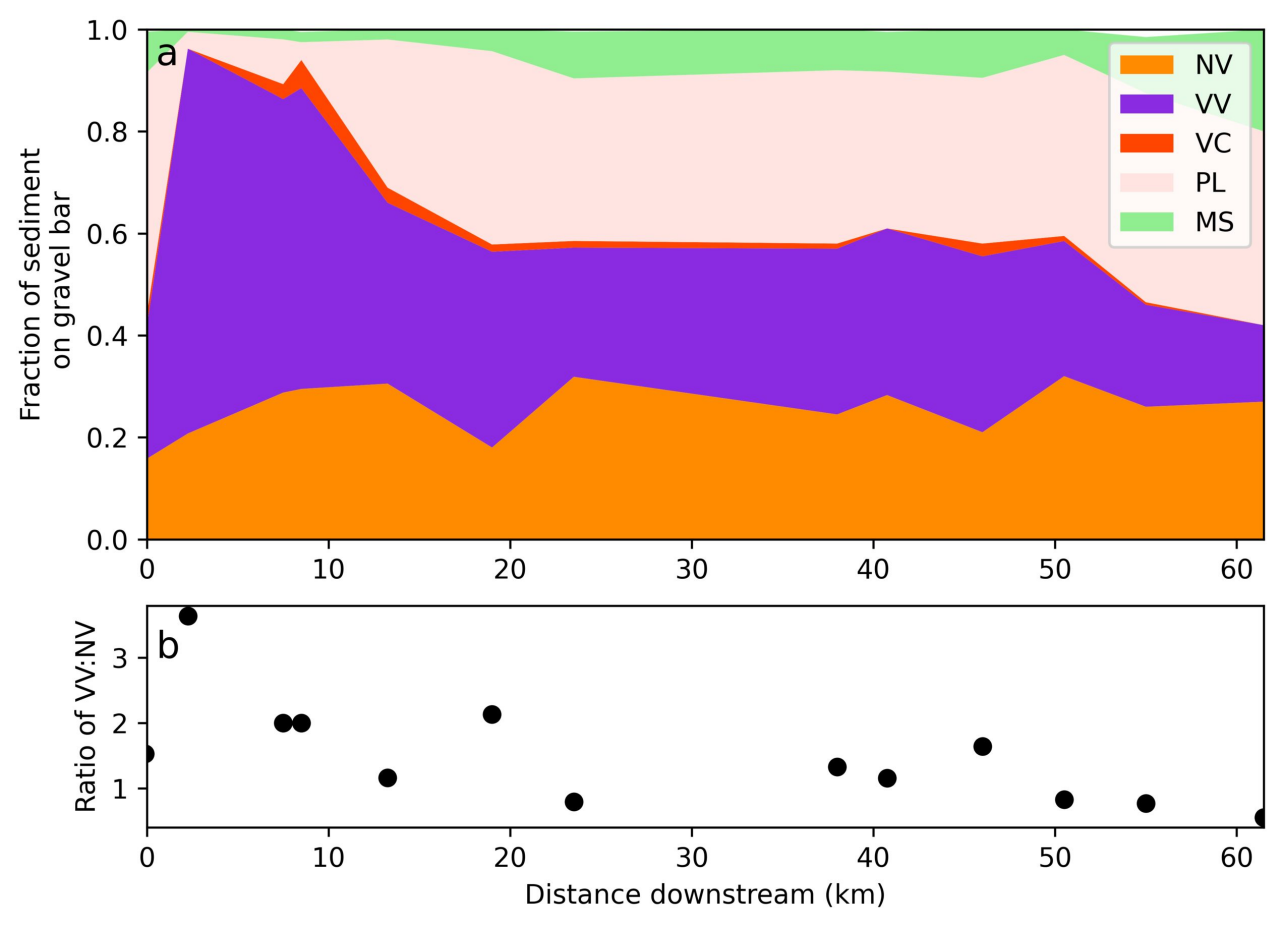
a
b
NV
VV
VC
PL
MS
Fraction of sediment on gravel bar
Ratio of VV:NV
Distance downstream (km)
0.0
0.2
0.4
0.6
0.8
1.0
1
2
3
0
10
20
30
40
50
60

Figure 8.

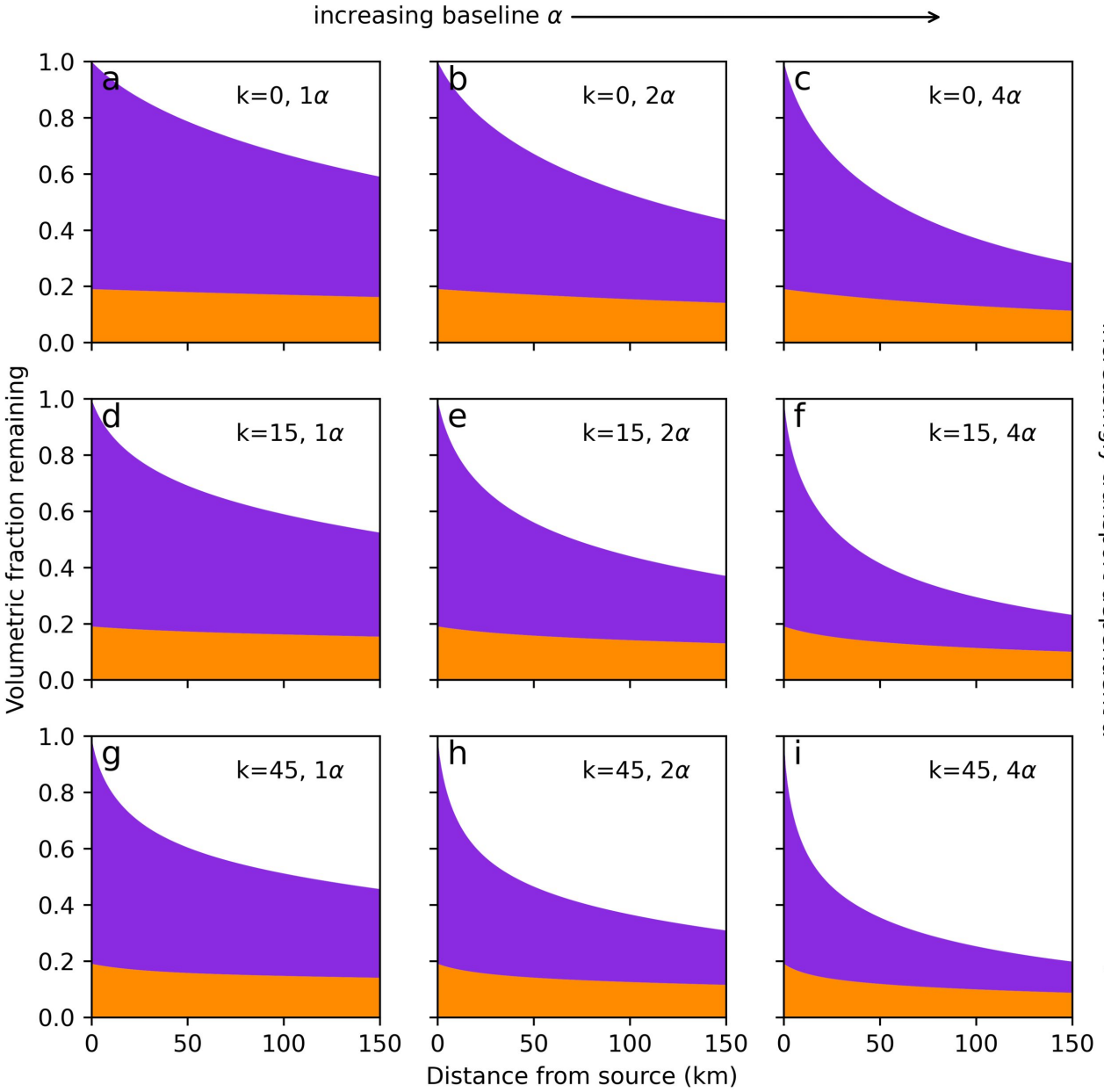
increasing baseline α
a
k=0, 1α
b
k=0, 2α
c
k=0, 4α
d
k=15, 1α
e
k=15, 2α
f
k=15, 4α
g
k=45, 1α
h
k=45, 2α
i
k=45, 4α
Volumetric fraction remaining
Distance from source (km)
increasingly transport-dependent α
0.0
0.2
0.4
0.6
0.8
1.0
0
50
100
150

Figure 9.

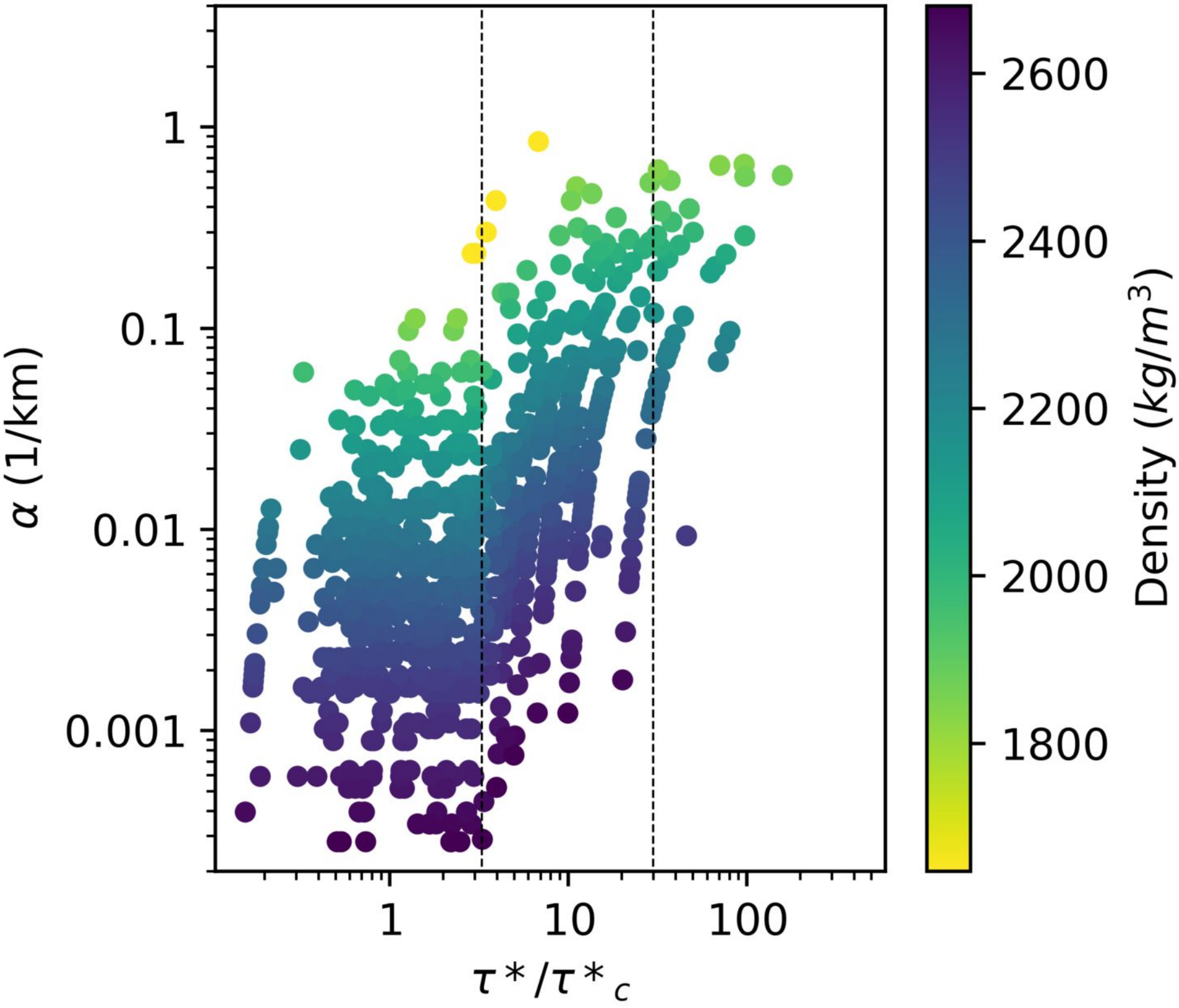
1
0.1
0.01
0.001
α (1/km)
1
10
100
τ*/τ*c
2600
2400
2200
2000
1800
Density (kg/m3)